Quaternary Science Reviews 28 (2009) 1171–1187

Contents lists available at ScienceDirect

Quaternary Science Reviews

journal homepage: www.elsevier.com/locate/quascirev

Latest Pleistocene glacial chronology of the Uinta Mountains: support for moisture-driven asynchrony of the last deglaciation

Benjamin J.C. Laabs [a,*], Kurt A. Refsnider [b,1], Jeffrey S. Munroe [c], David M. Mickelson [b], Patrick J. Applegate [d], Brad S. Singer [b], Marc W. Caffee [e]

[a] Department of Geological Sciences, SUNY Geneseo, 1 College Circle, Geneseo, NY 14454, United States
[b] Department of Geology and Geophysics, University of Wisconsin-Madison, 1215 W. Dayton St., Madison, WI 53716, United States
[c] Department of Geology, Middlebury College, 276 Bicentennial Way, Middlebury, VT 05753, United States
[d] Department of Geosciences, Penn State University, 532 Deike Building, University Park, PA 16802, United States
[e] Department of Physics, PRIME Lab, Purdue University, 525 Northwestern Avenue, West Lafayette, IN 47906, United States

ARTICLE INFO

Article history:
Received 25 July 2008
Received in revised form
9 December 2008
Accepted 10 December 2008

ABSTRACT

Recent estimates of the timing of the last glaciation in the southern and western Uinta Mountains of northeastern Utah suggest that the start of ice retreat and the climate-driven regression of pluvial Lake Bonneville both occurred at approximately 16 cal. ka. To further explore the possible climatic relationship of Uinta Mountain glaciers and the lake, and to add to the glacial chronology of the Rocky Mountains, we assembled a range-wide chronology of latest Pleistocene terminal moraines based on seventy-four cosmogenic ^{10}Be surface-exposure ages from seven glacial valleys. New cosmogenic-exposure ages from moraines in three northern and eastern valleys of the Uinta Mountains indicate that glaciers in these parts of the range began retreating at 22–20 ka, whereas previously reported cosmogenic-exposure ages from four southern and western valleys indicate that ice retreat began there between 18 and 16.5 ka. This spatial asynchrony in the start of the last deglaciation was accompanied by a 400-m east-to-west decline in glacier equilibrium-line altitudes across the Uinta Mountains. When considered together, these two lines of evidence support the hypothesis that Lake Bonneville influenced the mass balance of glaciers in southern and western valleys of the range, but had a lesser impact on glaciers located farther east. Regional-scale variability in the timing of latest Pleistocene deglaciation in the Rocky Mountains may also reflect changing precipitation patterns, thereby highlighting the importance of precipitation controls on the mass balance of Pleistocene mountain glaciers.

1. Introduction

The Uinta Mountains of northeastern Utah contain abundant geologic evidence of Quaternary glaciations (Atwood, 1909; Bradley, 1936; Osborn, 1973; Bryant, 1992; Oviatt, 1994; Laabs and Carson, 2005; Munroe, 2005; Refsnider et al., 2007). The crest of the range is oriented east–west, with many broad north- and south-trending valleys. In the western part of the range, valleys were occupied by outlet glaciers draining a broad ice field, whereas valleys east of this area were occupied by discrete valley glaciers (Fig. 1; Refsnider et al., 2007; Munroe and Laabs, in press). This pattern of glaciation has been attributed to a west-east decrease in snowfall during the last glaciation (Munroe et al., 2006; Laabs et al., 2006; Refsnider et al., 2008), a trend that also occurs in the range today (Fig. 2). The last glaciation in the Uinta Mountains was termed the Smiths Fork Glaciation by Bradley (1936) and was correlated with the Pinedale Glaciation elsewhere in the Rocky Mountains (Richmond and Fullerton, 1986). The glacial record of this and previous glaciations includes well-preserved sequences of moraines contained within canyons or on the piedmont, which mark the termini of glaciers and provide abundant material suitable for cosmogenic-exposure dating.

Recent studies provide the first numerical age controls on the Smiths Fork Glaciation. Rosenbaum and Heil (in press) recognize glacial flour in sediments delivered to Bear Lake (Utah and Idaho) by Bear River, which heads in the northwestern Uinta Mountains. Radiocarbon-age limits indicate the onset of glaciation in the Bear River drainage at ca 26 cal. ka, and a maximum influx of glacial flour

* Corresponding author. Tel.: +1 585 245 5305; fax: +1 585 245 5116.
E-mail addresses: laabs@geneseo.edu (B.J.C. Laabs), kurt.refsnider@colorado.edu (K.A. Refsnider), jmunroe@middlebury.edu (J.S. Munroe), davem@geology.wisc.edu (D.M. Mickelson), papplega@geosc.psu.edu (P.J. Applegate), bsinger@geology.wisc.edu (B.S. Singer), mcaffee@physics.purdue.edu (M.W. Caffee).
[1] Current address: Institute of Arctic and Alpine Research, University of Colorado – Boulder, 1560, 30th Street, 450 UCB, Boulder, CO 80303, United States.

0277-3791/$ – see front matter © 2008 Elsevier Ltd. All rights reserved.
doi:10.1016/j.quascirev.2008.12.012

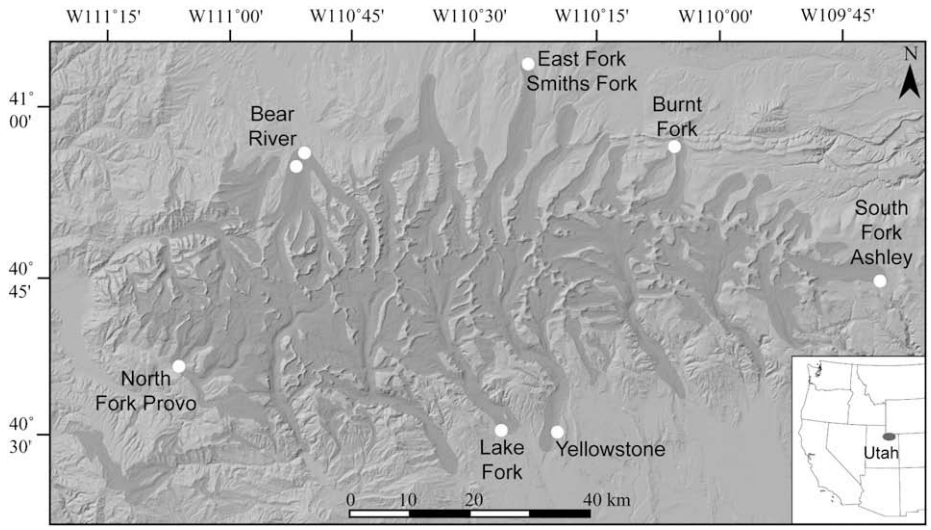

Fig. 1. Location map of the Uinta Mountains in the western United States (inset) and shaded-relief map of the glaciated portion of the Uinta Mountains. Ice extents of the Smiths Fork Glaciation (shaded gray) are from Munroe and Laabs (in press), Refsnider et al. (2007), Laabs and Carson (2005), Munroe (2005), and Oviatt (1994). Dots show general locations of moraine-boulder sampling areas for cosmogenic ^{10}Be surface-exposure dating.

at 20–19 cal. ka. Based on cosmogenic ^{10}Be surface-exposure dating of terminal moraines, Munroe et al. (2006) and Refsnider et al. (2008) infer that glaciers in southwestern valleys persisted at or near their maxima until about 17–16 ka, and Laabs et al. (2007a) determine that ice in a northwestern valley abandoned its terminal moraine at about 18 ka. These findings verify the culmination of the Smiths Fork Glaciation during Marine Oxygen Isotope Stage (MIS) 2 (e.g., Imbrie et al., 1984) and its correlation to the Pinedale Glaciation elsewhere in the Rocky Mountains (Richmond and Fullerton, 1986).

Cosmogenic-exposure age limits indicate that the start of deglaciation in the western Uinta Mountains was synchronous with the 16-cal.-ka hydrologic fall of Lake Bonneville, a large pluvial lake (surface area $>$ 50,000 km^2) that was located about 50 km west of the upwind end of the Uinta Mountains (Oviatt, 1997; Fig. 3). Munroe et al. (2006) infer a potential climatic link between the lake and Uinta Mountain glaciers, based on this synchrony and an eastward rise in reconstructed glacier equilibrium-line altitudes of 600 m across the Wasatch and Uinta Mountains (with 400 m of this rise occurring across the Uinta Mountains) during the Pinedale/Smiths Fork Glaciation. They propose that Lake Bonneville amplified precipitation over the Wasatch and western Uinta Mountains, steepening the west–east orographic precipitation gradient across these two mountain ranges.

Viewed at a regional scale, deglaciation in the western part of the Uinta Mountains began as much as 4 kyr later than in mountain ranges elsewhere in the Middle Rocky Mountains (Fig. 3), including the Wind River Range (Gosse et al., 1995) and several ranges in Colorado (Benson et al., 2005; Brugger, 2007). This apparent asynchrony may reflect regional differences in climate (e.g., Gillespie and Molnar, 1995), or differences in the primary controls of glacier mass balance (precipitation versus temperature) between mountain ranges (e.g., Thackray, 2008). However, some authors have highlighted the challenges of determining the accuracy of cosmogenic-exposure ages of moraine boulders, noting that apparent exposure-age variability can be due to moraine degradation/boulder exhumation, inherited cosmogenic nuclides, and shielding of moraine boulders by snow cover (e.g., Putkonen and Swanson, 2003; Benson et al., 2005; Ivy-Ochs et al., 2007). Continued improvement of the Pleistocene glacial chronology in this region is necessary to better understand late Quaternary climatic changes and to further develop cosmogenic-exposure dating and other chronological methods of dating glacial deposits.

In this paper, we greatly expand upon existing cosmogenic-exposure age data in the Uinta Mountains, presenting a range-wide chronology of terminal moraines of the Smiths Fork Glaciation based on cosmogenic ^{10}Be exposure dating in seven valleys. This spatially distributed and data-rich approach to developing a glacial chronology for the entire range is advantageous for several reasons. First, the systematic uncertainty inherent in estimating production rates of cosmogenic nuclides can be assumed equal for all cosmogenic-exposure ages within the Uinta Mountains because moraine-boulder samples are from a relatively narrow range of elevations (2319–2993 m asl) and geographic latitudes (N40.5°–N41.1°). Therefore, any significant variability among exposure ages of different Smiths Fork terminal moraines from one valley to the next can be explained by climatic, hypsometric, or exposure-history differences. Second, the excellent preservation of moraines in the Uinta Mountains affords the opportunity to identify such variability and to test the hypothesis that glaciers at the eastern end of the range, most distant from Lake Bonneville, were less influenced by the lake than those at the wetter, upwind end of the range. We evaluate this possibility by reporting and interpreting cosmogenic-exposure ages from moraines in three previously undated valleys in the northern and eastern parts of the range; the Smiths Fork, Burnt Fork, and South Fork Ashley Creek valleys (Fig. 1). In these valleys, glacier ELAs were ca 3100–3200 m asl during the Smiths Fork maximum (Munroe, 2005) compared to ELAs of 2800–3000 m asl for glaciers in western valleys (Shakun, 2003; Laabs and Carson, 2005; Refsnider et al., 2008). Finally, the apparent spatial variability in the timing of the last deglaciation in the Rocky Mountains has been attributed to changing precipitation patterns accompanying retreat of North American ice sheets in the western U.S. (e.g., Licciardi et al., 2004; Thackray et al., 2004). The Uinta Mountains are centrally located among other well-dated glacial settings in this region. Thus, refining the chronology here will improve the framework for understanding latest Pleistocene climate changes.

2. Cosmogenic-exposure dating methods

2.1. Moraine-boulder sampling

To build upon existing glacial chronologies for the Uinta Mountains, we targeted the best preserved moraines previously

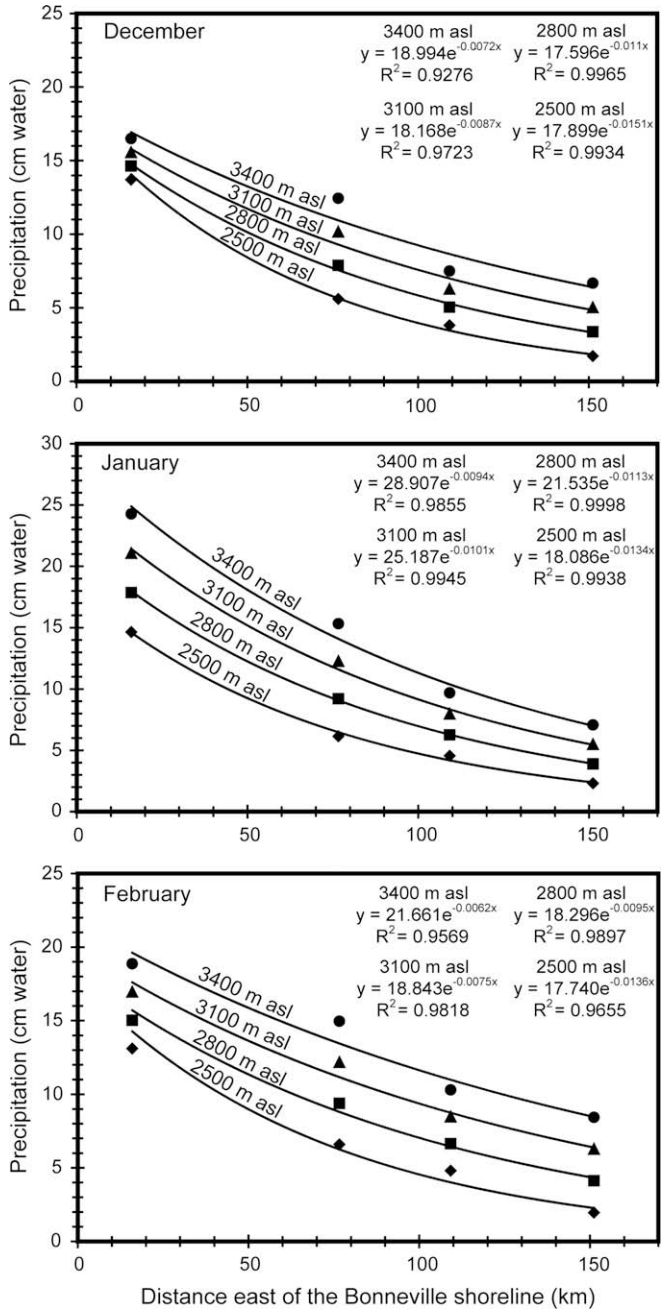

Fig. 2. West–east precipitation gradients across the Wasatch and Uinta Mountains at 2500, 2800, 3100, and 3400 m asl. Points are computed from extrapolated precipitation-elevation gradients determined from fifteen snowpack-telemetry (SNOTEL) stations in four valleys in the Wasatch and Uinta Mountains. Best-fit curves are exponential functions, with expressions and *R*-squared values noted in the upper right of each graph.

mapped as Smiths Fork in age (Refsnider et al., 2007; Munroe and Laabs, in press). In each valley, terminal moraines are prominent topographic features forming latero-frontal ridges (Fig. 4) and contain abundant boulders suitable for cosmogenic-exposure dating.

On each terminal-moraine complex, we sampled as many as fifteen boulders to evaluate the variability of cosmogenic-exposure ages. Boulders were selected for sampling based on several criteria. First, we sampled only boulders composed of weakly metamorphosed sandstone and quartzite of the Proterozoic Uinta Mountain Group, a lithology that is resistant to surface erosion and composed almost entirely of quartz. Second, we sampled (with rare exception) only boulders with tops more than 0.5 m above the moraine crest to minimize potential complications related to cosmic-ray shielding by snow and/or sediment cover. Last, boulders with clear evidence of surface weathering or erosion (e.g., rough surfaces with cm-scale weathering features), spallation, or overturning were avoided. Almost all sampled boulders were broad-based and had flat or gently rounded upper surfaces. In addition, most sampled boulders displayed glacial polish; on some boulders, striae were still preserved. The presence of such features easily removed by weathering suggests that the effect of boulder erosion on ^{10}Be concentrations in our samples is minimal.

2.2. Sampling preparation and analysis

Samples were prepared for beryllium-isotope analysis following methods modified from Bierman et al. (2002) in the University of Wisconsin Cosmogenic Nuclide Preparation Laboratory (Munroe et al., 2006). At least 20–50 g of purified quartz were separated from each boulder sample, dissolved, spiked with approximately 500 μg of SPEX-brand commercial-grade ^{9}Be solution (1 mg/L) and processed to chemically isolate beryllium. Ratios of ^{10}Be/^{9}Be were determined by accelerator mass spectrometry (AMS) at the Purdue University PRIME Lab (Muzikar et al., 2003). All measured ratios used for age calculations were first corrected for measured ^{10}Be/^{9}Be in sample blanks, an adjustment that for nearly all samples was less than 4%.

2.3. Age calculations

All new and previously reported cosmogenic-exposure ages from the Uinta Mountains were computed (or recomputed) based on measured ^{10}Be/^{9}Be ratios and the ^{10}Be exposure-age calculation scheme of Balco et al. (2008), using the CRONUS-Earth online exposure-age calculator (available at http://hess.ess.washington.edu/math/). We used version 2.0 of the calculator, which computes exposure ages based on a sea-level, high-latitude, spallogenic production rate of 4.96 ± 0.43 (1σ) atoms g SiO_2^{-1} yr^{-1}; scaled for sample thickness, topographic shielding (if necessary), site elevation, and latitude based on models for a constant or time-dependent production rate. This version of the calculator also includes a muonic production-rate model from Heisinger et al. (2002a,b).

We report only ages computed by a constant-production-rate model that combines scaling schemes for elevation and geographic latitude of Lal (1991) and Stone (2000). This model is appropriate because the estimated production rate incorporates the effects of variations in the Earth geomagnetic field and the position of the dipole axis over the past ~20 ka (Gosse and Phillips, 2001). Although the systematic uncertainty of calculating site-specific production rates may be as much as 20% (Desilets and Zreda, 2001), we incorporate only the 1σ uncertainty of AMS analysis into each age estimate (see Table 1) for the purpose of comparing cosmogenic-exposure ages in the Uinta Mountains with one another and with others from elsewhere in the Rocky Mountain region.

3. Cosmogenic-exposure ages in the Uinta Mountains

Cosmogenic-exposure ages from seven terminal-moraine complexes in the Uinta Mountains are summarized in Table 1 and Figs. 5 and 6. Table 1 and Fig. 5 report both the mean of the cosmogenic-exposure ages and the oldest age from each moraine; Fig. 6 shows our preferred estimate of the time of terminal-moraine abandonment (either the mean or the oldest exposure age) in each valley. In this section, we describe our overall interpretive scheme.

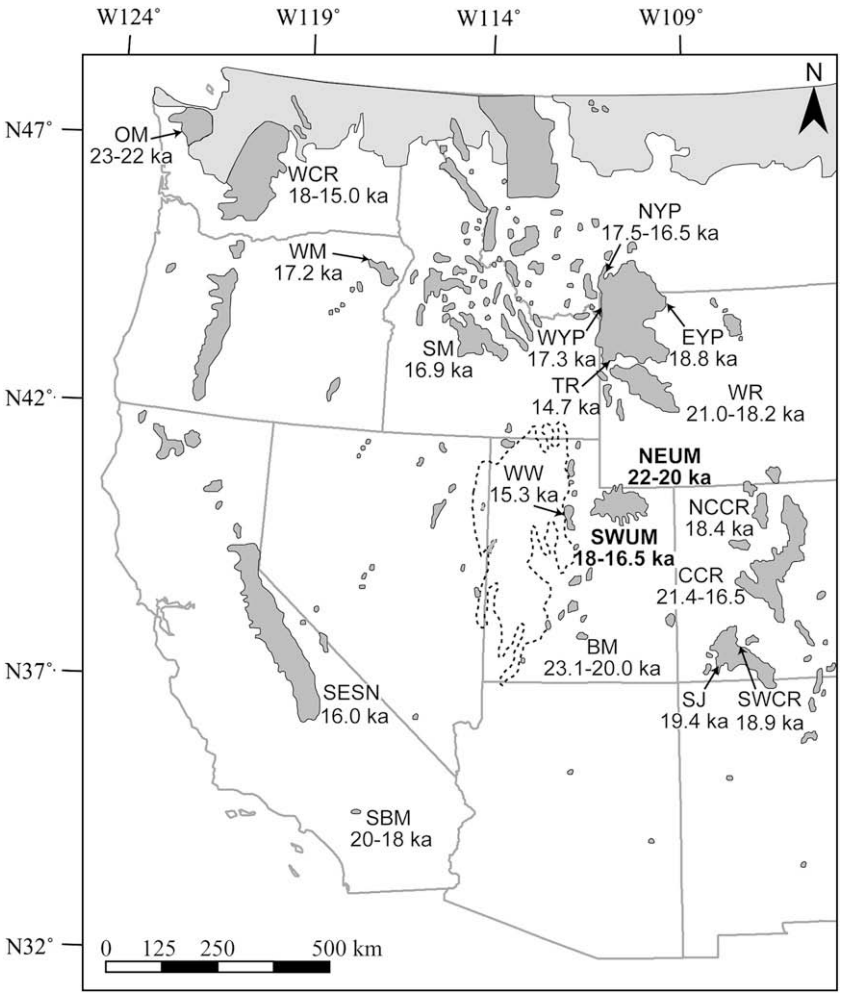

Fig. 3. Generalized ice extents of the LGM in the conterminous western United States (after Porter et al., 1983) and age limits on the start of terminal-moraine abandonment (uncertainties of age estimates are not shown, but are included in the text; see Section 4). Age limits for the Olympic Mountains (OM) are from Thackray (2001); the Washington Cascade Range (WCR) are from Porter et al. (2008); the Wallowa Mountains (WM) are from Licciardi et al. (2004); the Sawtooth Range (SR) are from Thackray et al. (2004); the northern, western, and eastern Yellowstone Plateau (NYP, WYP, EYP, respectively) and Teton Range (TR) are from Licciardi and Pierce (2008); the Wind River Mountains (WM) are from Benson et al. (2005); the western Wasatch Mountains (WW) are from Laabs et al. (2007b); the southwestern and northeastern Uinta Mountains (SWUM and NEUM, respectively) are from Munroe et al. (2006), Laabs et al. (2007a), Refsnider et al. (2008) and this study; the north-central and southwestern Colorado Rocky Mountains (NCCR, SWCR respectively) are from Benson et al. (2005); the central Colorado Rocky Mountains (CCR) are from Brugger (2007); the San Juan Mountains (SJ) are from Guido et al. (2007); the central Colorado Plateau at Boulder Mountain (BM) are from Marchetti et al. (2005); the San Bernadino Mountains (SB) are from Owen et al. (2003); the southeastern Sierra Nevada (SESN) are from Phillips et al. (1996). Cosmogenic ^{10}Be surface-exposure ages of Benson (2005, WR only) have been recalculated using Balco et al. (2008). Dashed line shows the extent of pluvial Lake Bonneville, which attained its highstand from about 19 to 17 cal. ka (Oviatt, 1997).

In Sections 3.1–3.7, we discuss our treatment of the cosmogenic-exposure ages from each moraine in more detail.

There are several approaches to interpreting cosmogenic-exposure ages of moraine boulders described in the literature. Some workers believe the best estimate of moraine age is the average of exposure ages, perhaps after excluding statistical outliers (e.g., Kaplan et al., 2005); others prefer the oldest among a set of exposure ages (e.g., Briner et al., 2005) or the youngest (e.g., Benson et al., 2005). This variety of interpretive methods stems from the observed scatter of exposure ages from individual moraines, which is often larger than can be explained by measurement error. On average, cosmogenic-exposure data sets from latest Pleistocene moraines (within the range of 24–12 ka) display a range of ca 40% of the oldest cosmogenic-exposure age even after old outliers are excluded (Putkonen and Swanson, 2003; Balco and Schaefer, 2006). Additionally, cosmogenic-exposure ages from individual moraines are often not symmetrically distributed about their means. Such distributions may reflect moraine-crest erosion by hill-slope processes that occur rapidly after the start of ice retreat, and continue more slowly through time. This behavior is consistent with field observations on moraines (e. g., Putkonen et al., 2008), and has been reproduced by numerical models of landform evolution (e.g., Hallet and Putkonen, 1994). However, broad scatter of cosmogenic-exposure ages can also result from the presence of inherited nuclides in moraine boulders (e.g., Benson et al., 2005). Evaluating the relative effects of moraine degradation and inheritance on cosmogenic-exposure ages can be difficult; many authors assert that the latter effect is minimal based on the assumption that the depth of glacial erosion and clast-size reduction during glacial transport were sufficient to remove any inherited nuclides.

Following Applegate et al. (2008), we suggest that the statistical distribution of cosmogenic-exposure ages from a single moraine can be used to infer the cause of exposure-age variability and, ultimately, indicate whether the mean or the oldest of a set of exposure ages best represents the time of moraine abandonment. In cases where the observed distribution of cosmogenic-exposure ages is skewed, using the mean or the weighted mean of exposure

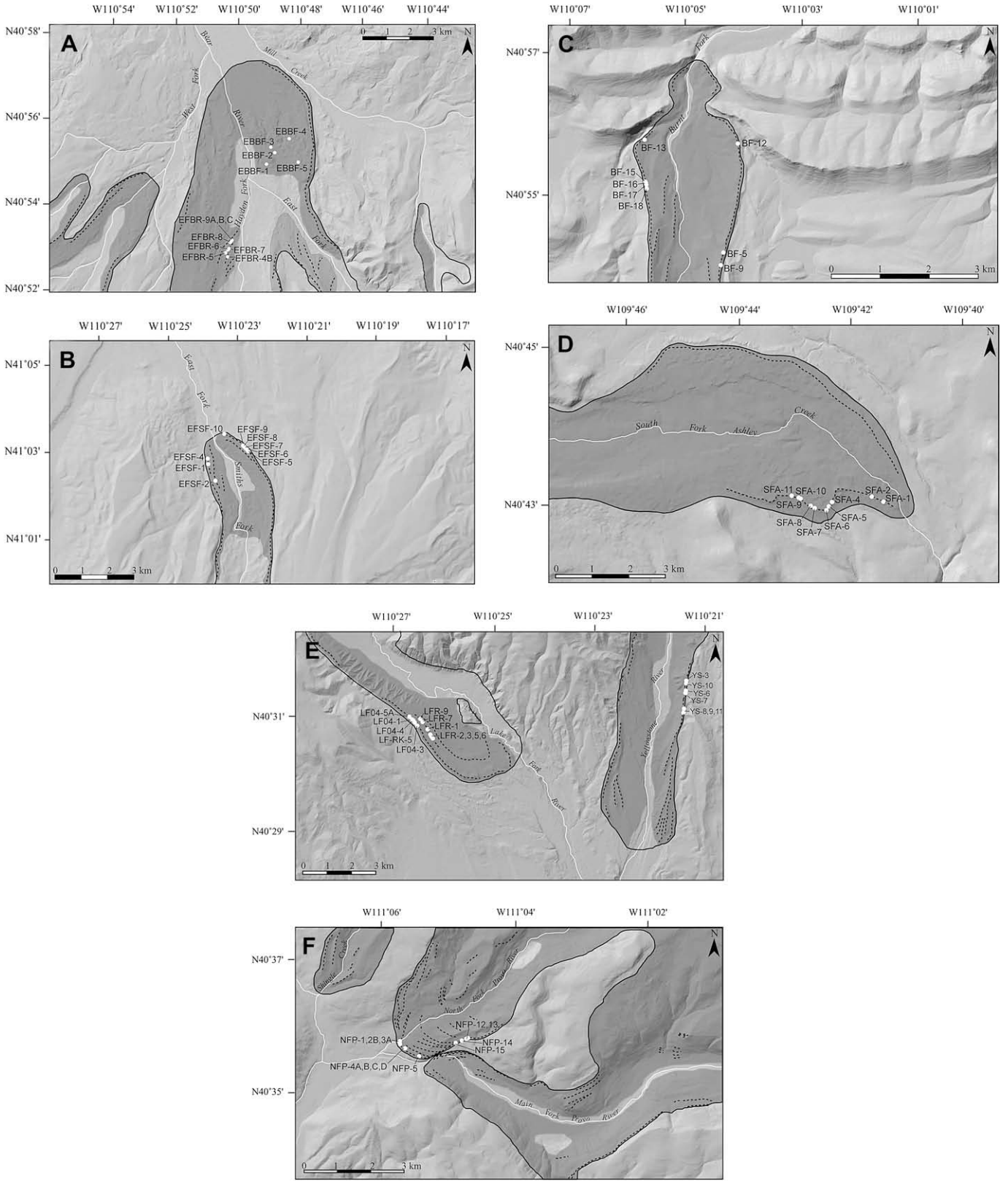

Fig. 4. Shaded-relief maps of moraines in the Bear River (A), East Fork Smiths Fork (B), Burnt Fork (C), South Fork Ashley Creek (D), Lake Fork/Yellowstone Rivers (E) and North Fork Provo River (F) valleys. Black lines indicate ice extents of the Smiths Fork Glaciation, shaded gray areas indicate mapped extent of till (from Refsnider et al., 2007; Munroe and Laabs, in press), dashed lines indicate moraine crests, and white dots indicate locations of moraine boulders sampled for cosmogenic-exposure dating (see Table 1 for cosmogenic-exposure ages).

Table 1
^{10}Be data and cosmogenic-exposure ages for Uinta Mountain moraines.

Sample locale[a]	Sample Id[b]	Elevation (m asl)	Latitude (N)	Longitude (W)	Boulder height (m)	^{10}Be/^{9}Be	1σ	[^{10}Be] (atoms g SiO_2^{-1})	1σ	Sample thickness (cm)	Topographic shielding factor	Production rate[d]	Stone (2000)/ Lal (1991) CRONUS-Earth exposure age (ka)[d]	1σ[e] (kyr)	Stone (2000) exposure age (ka)[f]	1σ[e] (kyr)
North slope																
Bear River																
Distal area	EBBF-1	2646	40.9178	−110.8210	0.95	6.84E−13	3.75E−14	5.48E+05	3.00E+04	4.5	1	33.28	16.3	0.9	16.6	0.9
	EBBF-2	2640	40.9224	−110.8210	0.95	7.05E−13	3.46E−14	5.83E+05	2.86E+04	6.5	1	31.65	18.2	0.9	18.6	0.9
	EBBF-3	2654	40.9241	−110.8210	0.95	6.86E−13	1.91E−14	5.34E+05	1.48E+04	6.5	1	31.63	16.7	0.5	17.0	0.5
	EBBF-4	2654	40.9280	−110.8210	1.00	7.79E−13	4.25E−14	5.70E+05	3.11E+04	3.5	1	32.13	17.6	1.0	17.9	1.0
	EBBF-5	2654	40.9181	−110.8210	1.50	7.93E−13	4.74E−14	6.24E+05	3.73E+04	4.5	1	33.26	18.6	1.1	18.9	1.1
												Mean ± 1σ ($n = 5$) = 17.5 ± 1.0; oldest boulder = 18.6 ± 1.1				
Proximal area	EFBR-4A	2640	40.8788	−110.8417	0.55	9.82E−13	1.80E−13	7.29E+05	1.34E+05	4.5	1	33.13	21.8[g]	4.0	22.2[g]	4.1
	EFBR-4B	2640	40.8788	−110.8417	0.86	8.94E−13	3.43E−14	6.46E+05	2.47E+04	4.0	1	33.26	19.2	0.7	19.6	0.8
	EFBR-5	2651	40.8805	−110.8429	1.30	8.25E−13	3.65E−14	6.44E+05	2.85E+04	5.0	1	33.22	19.2	0.9	19.6	0.9
	EFBR-7	2646	40.8822	−110.8409	0.62	8.60E−13	8.01E−14	6.41E+05	5.97E+04	3.0	1	33.67	18.9	1.8	19.2	1.8
	EFBR-8	2640	40.8847	−110.8403	0.87	8.42E−13	2.97E−14	6.45E+05	2.28E+04	4.5	1	33.13	19.3	0.7	19.7	0.7
	EFBR-9A	2654	40.8855	−110.8394	0.87	7.87E−13	3.46E−14	5.92E+05	2.60E+04	5.0	1	33.29	17.6	0.8	17.9	0.8
	EFBR-9B	2654	40.8855	−110.8394	1.47	9.36E−13	5.34E−14	7.13E+05	4.06E+04	4.5	1	33.43	21.1	1.2	21.5	1.2
	EFBR-9C	2654	40.8855	−110.8394	0.86	7.90E−13	3.59E−14	5.76E+05	2.62E+04	5.0	1	33.29	17.1	0.8	17.5	0.8
												Mean ± 1σ ($n = 7$) = 18.9 ± 1.3; oldest boulder = 21.1 ± 1.2				
East Fork	EFSF-1	2692	41.0442	−110.4016	0.45	2.36E−12	1.00E−12	1.69E+06	7.18E+05	7.0	1	33.63	50.1[g]	21.6	51.3[g]	22.0
Smiths Fork	EFSF-2	2714	41.0381	−110.3972	0.85	8.80E−13	6.01E−14	6.44E+05	4.40E+04	2.0	1	35.63	18.0	1.2	18.3	1.3
	EFSF-4	2741	41.0463	−110.3983	0.35	9.60E−13	3.68E−14	7.12E+05	2.73E+04	5.0	1	35.26	20.0	0.8	19.5	0.8
	EFSF-5	2727	41.0493	−110.3813	0.54	7.77E−13	3.82E−14	5.64E+05	2.78E+04	6.0	1	34.67	16.1	0.8	16.4	0.8
	EFSF-6	2718	41.0496	−110.3814	0.40	1.64E−12	4.80E−13	1.17E+06	3.44E+05	5.0	1	34.76	33.5[g]	9.9	34.2[g]	10.1
	EFSF-7	2715	41.0503	−110.3818	0.50	1.42E−12	8.01E−14	1.09E+06	6.13E+04	3.0	1	35.26	30.7[h]	1.7	31.1[h]	1.8
	EFSF-8	2713	41.0508	−110.3823	0.40	1.02E−12	4.92E−14	7.61E+05	3.68E+04	4.0	1	34.93	21.6	1.1	22.0	1.1
	EFSF-9	2700	41.0511	−110.3826	0.45	2.36E−12	1.70E−13	1.80E+06	1.30E+05	4.0	1	34.65	51.9[h]	3.8	52.7[h]	3.8
	EFSF-10	2650	41.0558	−110.3929	0.62	1.23E−12	5.42E−14	9.31E+05	4.10E+04	2.0	1	34.12	27.1	1.2	27.5	1.2
												Mean ± 1σ ($n = 4$) = 18.9 ± 2.4; oldest boulder = 21.6 ± 1.1				
Burnt Fork	BF-5	2958	40.9029	−110.0766	0.50	8.78E−13	2.30E−13	6.55E+05	1.72E+05	7.0	1	39.27	16.6[g]	4.4	16.8[g]	4.4
	BF-9	2993	40.8981	−110.0772	0.40	1.01E−12	9.04E−14	7.32E+05	6.56E+04	5.0	1	40.77	17.9	1.6	18.0	1.6
	BF-12	2779	40.9259	−110.0722	0.85	9.74E−13	4.08E−14	7.03E+05	2.95E+04	10.0	0.9960	34.34	20.5	0.9	20.7	0.9
	BF-13	2800	40.9245	−110.0934	0.47	6.75E−13	3.10E−14	4.91E+05	2.26E+04	5.0	0.9927	36.23	13.6	0.6	13.7	0.6
	BF-15	2812	40.9171	−110.0952	0.49	7.79E−13	3.88E−14	5.82E+05	2.90E+04	6.0	1	36.20	16.0	0.8	16.1	0.8
	BF-16	2840	40.9168	−110.0951	0.53	8.78E−13	6.05E−14	6.31E+05	4.35E+04	5.0	1	37.41	16.9	1.2	17.0	1.2
	BF-17	2826	40.9164	−110.0950	0.52	9.10E−13	4.18E−14	6.62E+05	3.04E+04	7.0	1	36.49	18.2	0.8	18.4	0.8
	BF-18	2835	40.9156	−110.0960	0.49	6.98E−13	1.20E−13	5.08E+05	8.77E+04	7.0	1	36.69	13.9[g]	13.2.4	14.0[g]	2.4
												Mean ± 1σ ($n = 5$) = 17.2 ± 2.3; oldest boulder = 20.5 ± 0.9				

South slope																
North Fork Provo																
Terminal	NFP-1	2319	40.5985	−111.0942	0.76	3.35E−13	1.62E−14	3.22E+05	1.56E+04	5.0	0.9997	26.63	11.9	0.6	12.2	0.6
Moraine	NFP-2B	2327	40.7023	−111.0945	0.69	4.62E−13	1.62E−14	4.35E+05	1.53E+04	3.0	0.9997	27.26	15.8	0.6	16.0	0.6
	NFP-3A	2321	40.7020	−111.0937	1.89	4.02E−13	4.31E−14	4.81E+05	5.16E+04	6.0	0.9997	26.49	18.0	1.9	18.3	2.0
	NFP-4A	2324	40.5965	−111.0927	1.25	7.23E−13	2.02E−14	4.73E+05	1.32E+04	5.0	0.9990	26.69	17.5	0.5	17.0	0.5
	NFP-4B	2324	40.5963	−111.0927	1.55	3.86E−13	1.92E−14	3.91E+05	1.94E+04	2.5	0.9995	27.26	14.2	0.7	14.4	0.7
	NFP-4C	2324	40.5963	−111.0927	0.83	3.66E−13	1.82E−14	3.75E+05	1.86E+04	3.0	0.9995	27.15	13.6	0.7	13.9	0.7
	NFP-4D	2324	40.5963	−111.0927	0.66	7.95E−13	3.81E−14	5.33E+05	2.55E+04	3.0	0.9990	27.14	19.4	0.9	19.2	0.9
	NFP-5	2346	40.5946	−111.0870	1.57	4.26E−13	1.62E−14	4.39E+05	1.18E+04	3.5	1	27.45	15.8	0.4	16.1	0.4
												Mean ± 1σ (*n* = 8) = 15.8 ± 2.5; oldest boulder = 19.4 ± 1.9				
Lateral Moraine	NFP-12	2505	40.6006	−111.0719	0.60	7.61E−13	2.31E−14	4.93E+05	1.50E+04	6.0	0.9995	29.85	16.3	0.5	15.7	0.5
	NFP-13	2504	40.6007	−111.0718	0.45	7.78E−13	2.31E−14	5.11E+05	1.52E+04	4.5	0.9995	30.19	16.7	0.5	16.3	0.5
	NFP-14	2489	40.6003	−111.0733	0.75	8.03E−13	2.21E−14	5.42E+05	1.49E+04	3.0	0.9995	30.27	17.7	0.5	17.5	0.5
	NFP-15	2471	40.5996	−111.0753	1.10	7.81E−13	2.61E−14	5.37E+05	1.80E+04	2.5	0.9995	30.04	17.7	0.6	17.5	0.6
												Mean ± 1σ (*n* = 4) = 17.1 ± 0.7; oldest boulder = 17.7 ± 0.6				
Lake Fork																
Distal Ridge	LF-RK-5	2551	40.5172	−110.4603	0.50	5.47E−13	3.00E−14	6.03E+05	3.77E+04	2.5	1	31.59	18.9	1.2	19.2	1.2
	LF04-1	2561	40.5166	−110.4615	0.64	7.02E−13	2.40E−14	5.16E+05	2.35E+04	5.0	1	31.15	16.4	0.8	16.7	0.8
	LF04-2	2560	40.5176	−110.4627	1.20	7.85E−13	2.30E−14	5.37E+05	2.25E+04	6.0	1	30.87	17.2	0.7	17.7	0.7
	LF04-3	2543	40.5144	−110.4584	0.35	5.20E−13	2.10E−14	3.40E+05	1.71E+04	3.0	1	31.29	10.7	0.5	11.5	0.6
	LF04-4	2555	40.5163	−110.4608	0.47	6.36E−13	2.60E−14	6.04E+05	3.06E+04	7.0	1	30.53	19.6	1.0	19.9	1.0
	LF04-5A[j]	2555	40.5172	−110.4623	0.48	6.42E−13	2.00E−14	5.54E+05	2.40E+04	8.0	1	30.28	18.1	0.8	18.4	0.8
	LF04-5B[j]	2555	40.5172	−110.4623	0.56	6.21E−13	2.10E−14	5.54E+05	2.50E+04	4.0	1	31.28	17.5	0.8	17.8	0.8
												Mean ± 1σ (*n* = 7) = 16.9 ± 2.9; oldest boulder = 19.6 ± 1.0				
Proximal Ridge	LFR-1	2464	40.5131	−110.4533	0.68	6.22E−13	2.00E−14	5.09E+05	2.24E+04	1.0	1	30.22	16.7	0.7	17.1	0.8
	LFR-3	2464	40.5112	−110.4519	0.71	6.98E−13	3.50E−14	5.34E+05	3.12E+04	2.0	1	29.97	17.6	1.0	18.0	1.1
	LFR-4	2464	40.5105	−110.4515	0.51	7.28E−13	3.10E−14	4.87E+05	2.54E+04	2.0	1	29.97	16.1	0.8	16.6	0.9
	LFR-5	2464	40.5103	−110.4511	0.65	5.95E−13	5.00E−14	4.69E+05	4.18E+04	8.0	1	28.54	16.3	1.5	16.7	1.5
	LFR-6	2464	40.5098	−110.4509	0.61	5.89E−13	2.60E−14	4.70E+05	2.51E+04	7.0	1	28.77	16.2	0.9	16.1	0.9
	LFR-7	2464	40.5157	−110.4560	0.70	6.61E−13	2.50E−14	5.07E+05	2.45E+04	2.5	1	29.85	16.8	0.8	16.7	0.8
	LFR-9	2464	40.5167	−110.4572	0.50	6.41E−13	2.60E−14	5.05E+05	2.55E+04	2.5	1	29.85	16.7	0.8	16.6	0.8
												Mean ± 1σ (*n* = 7) = 16.6 ± 0.5, oldest boulder = 17.6 ± 1.0				

(*continued on next page*)

Table 1 (*continued*)

Sample locale[a]	Sample Id[b]	Elevation (m asl)	Latitude (N)	Longitude (W)	Boulder height (m)	$^{10}Be/^{9}Be$	1σ	[^{10}Be] (atoms g SiO_2^{-1})	1σ	Sample thickness (cm)	Topographic shielding factor	Production rate[d]	Stone (2000)/ Lal (1991) CRONUS-Earth exposure age (ka)[d]	1σ[e] (kyr)	Stone (2000) exposure age (ka)[f]	1σ[e] (kyr)
Yellowstone	YS-3	2561	40.5324	−110.3256	1.20	5.83E−13	2.00E−14	5.53E+05	2.52E+04	2.5	1	31.80	17.2	0.8	17.4	0.8
	YS-6	2540	40.5291	−110.3262	0.50	4.59E−13	1.30E−14	4.00E+05	1.65E+04	7.0	1	30.23	13.0	0.5	13.3	0.6
	YS-7	2531	40.5282	−110.3262	0.60	4.91E−13	1.40E−14	4.61E+05	1.91E+04	5.0	1	30.55	14.9	0.6	15.1	0.6
	YS-8	2517	40.5223	−110.3270	0.80	6.66E−13	1.60E−14	5.86E+05	2.25E+04	2.5	1	30.90	18.7	0.7	19.0	0.7
	YS-9	2514	40.5207	−110.3272	1.00	5.57E−13	1.70E−14	5.36E+05	2.29E+04	2.5	1	30.84	17.2	0.7	17.4	0.8
	YS-10	2554	40.5317	−110.3258	0.60	6.40E−13	1.90E−14	5.63E+05	2.38E+04	2.5	1	31.65	17.6	0.7	17.9	0.8
	YS-11	2512	40.5208	−110.3271	0.35	3.50E−13	1.00E−14	3.50E+05	1.45E+04	9.0	1	29.21	11.8	0.5	12.0	0.5
												Mean ± 1σ ($n = 7$) = 15.8 ± 2.6; oldest boulder = 18.7 ± 0.7				
South Fork Ashley	SFA-1	2854	40.7174	−109.6837	0.9	1.06E−12	2.63E−14	7.99E+05	1.98E+04	7.0	1	36.98	21.4	0.5	21.9	0.5
	SFA-2	2846	40.7189	−103.6873	1.22	1.23E−12	4.12E−14	8.80E+05	2.95E+04	7.0	1	37.05	23.6	0.8	24.2	0.8
	SFA-4	2913	40.7191	−109.6988	0.5	1.27E−12	3.28E−14	9.06E+05	2.34E+04	3.0	1	39.62	22.7	0.6	23.1	0.6
	SFA-5	2900	40.7175	−109.6999	0.9	1.10E−12	4.45	8.30E+05	3.35E+04	4.0	1	38.99	21.1	0.9	21.5	0.9
	SFA-6	2891	40.7163	−109.7010	0.95	2.99E−12	9.12E−14	2.21E+06	6.74E+04	2.0	1	39.41	56.1[h]	1.7	57.1[h]	1.8
	SFA-7	2921	40.7165	−109.7045	0.82	2.19E−12	5.26E−14	1.59E+06	3.82E+04	4.0	1	39.49	40.1[h]	1.0	41.0[h]	1.0
	SFA-8	2945	40.7176	−109.7057	0.52	1.15E−12	2.49E−14	8.51E+05	1.84E+04	8.0	1	38.79	21.8	0.5	22.2	0.5
	SFA-9	2949	40.7186	−109.7087	0.62	9.43E−13	3.80E−14	7.11E+05	2.87E+04	7.0	1	39.20	18.0	0.7	18.4	1.5
	SFA-10	2976	40.7189	−109.7090	0.55	1.15E−12	2.27E−14	8.51E+05	1.68E+04	2.0	1	41.52	20.3	0.4	20.7	0.4
	SFA-11	2969	40.7196	−109.7114	0.48	2.83E−12	1.24E−14	2.13E+05	9.36E+04	8.0	1	39.36	54.1[h]	2.4	55.3[h]	2.5
												Mean ± 1σ ($n = 7$) = 21.3 ± 1.9; oldest boulder = 23.6 ± 0.8				

Note: ages listed under the column heading "Stone (2000)/Lal (1991)" are consistent with those reported in the text.

[a] See locations and relief maps of moraine in Figs. 1 and 4.

[b] All samples are composed of quartzite or weakly metamorphosed sandstone and have a density of 2.65 g cm^{-3}.

[c] Ratios for samples from all valleys except the Lake Fork and Yellowstone were measured against ICN/Nishiizumi standards. Samples from the Lake Fork and Yellowstone valleys were measured against NIST standard SRM 4325, therefore ratios were increased by 14%. All ratios were corrected for sample blanks (an adjustment of less than 4% for nearly all samples).

[d] Spallogenic production-rate determined by CRONUS online exposure-age calculator, version 2.0 (Balco et al., 2008; http://hes.ess.washington.edu/math). The arithmetic mean is reported for each moraine. Uncertainty is 1σ of the distribution of acceptable cosmogenic-exposure dated from each moraine.

[e] Analytical uncertainty of AMS measurement.

[f] Computed using Stone (2000) production rate (sea-level, high-latitude = 5.1 ± 0.15 atoms g^{-1} SiO_2 yr^{-1}) and scaling scheme.

[g] The relatively great analytical and age uncertainty are due to loss of approximately 50% of sample mass during preparation of AMS targets; the age is not included in calculations of the mean cosmogenic-exposure age.

[h] Age predates the onset of the local LGM (ca 26 ka) as determined from radiocarbon-age limits on Bear Lake sediment (Rosenbaum and Heil, in press), suggesting that the boulder was reworked or that the moraine is a compound feature constructed during two separate glacial intervals.

[i] Age is an outlier not included in calculation of mean exposure age.

[j] Sampled LF04-5A, 5B were collected from different locations on a single boulder surface.

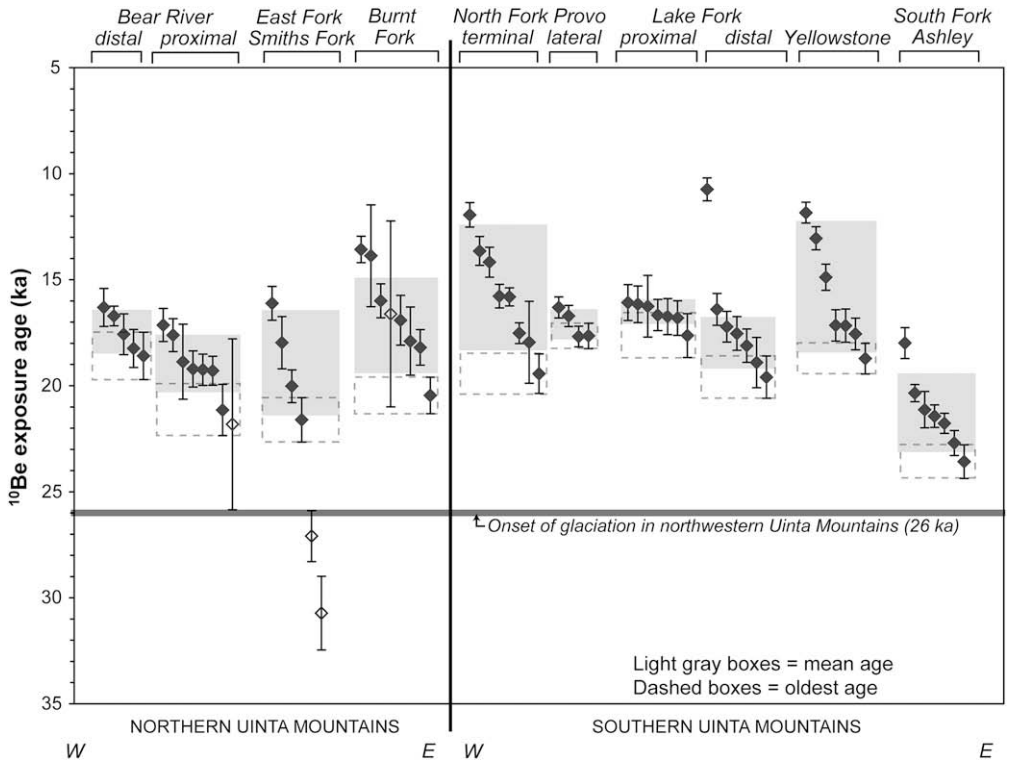

Fig. 5. Plot of all cosmogenic-exposure ages (less than 30 ka) of moraine boulders in the Uinta Mountains. Error bars are 1σ uncertainty of the AMS analysis. Open symbols indicate outliers not used for estimating moraine age. Gray boxes indicate the mean $\pm$ 1σ of acceptable cosmogenic-exposure ages, dashed boxes indicate the oldest cosmogenic-exposure age that post-dates 26 cal. ka, the onset of the last glaciation in the Uinta Mountains (from Rosenbaum and Heil, in press).

ages to estimate the age of a moraine may not be appropriate (Bevington and Robinson, 2002). Additionally, the oldest exposure age may not represent the true age of a moraine if inherited nuclides are abundant. However, as noted by Applegate et al. (2008), the skewness of an age distribution can reflect the dominant cause of exposure-age variability.

We use a numerical model of moraine degradation and cosmogenic-nuclide accumulation developed by Applegate et al. (2008) to aid in determining the best age estimate of moraine abandonment. Following Hallet and Putkonen (1994), the model assumes that moraines begin with a triangular cross-section with hill slopes at the angle of repose for diamicton (34°), and degrade from that initial condition by diffusive down-slope movement of material. The removal of material from the moraine crest causes the moraine to become shorter and more rounded (Fig. 7B). In the model, boulders are uniformly distributed throughout the moraine and come to the surface as material is removed from the moraine crest. The model tracks ^{10}Be concentrations in a large number of synthetic boulders, taking into account production due to both nucleons and muons (Granger and Muzikar, 2001).

Preliminary applications of the model reveal that moraine degradation tends to produce left-skewed distributions of exposure ages (Applegate et al., 2008). For example, consider the Yellowstone lateral moraine in the southwestern part of the range (Fig. 7, top left). In Fig. 7 (lower left), the exposure ages from the Yellowstone moraine are plotted as an empirical cumulative density function, along with a statistical distribution of apparent exposure ages from the model. The model curve passes within 1σ of all but one of the exposure ages. This model fit implies an age corresponding to the vertical, dashed line, suggesting that the true age of the Yellowstone moraine lies closest to the oldest age.

We take the oldest exposure age as the best estimate of moraine age in cases where we are able to produce a good fit between the model curve and the observed exposure dates. This condition is satisfied for the Yellowstone moraine and the ice-distal Lake Fork moraine (Fig. 7).

For moraines where we cannot produce a good fit between the model curve and our observations, we use the mean of the exposure ages to estimate moraine ages. We prefer the mean to the weighted mean (Bevington and Robinson, 2002) because the uncertainty of cosmogenic-exposure dating grows with the apparent age of the sample (Kaplan et al., 2005). Because the weighted mean gives preference to samples with small analytical uncertainty, this estimator of moraine age can be biased toward young values.

Estimating the true age of a moraine from data sets with old outliers can be more challenging, and in our case involves the treatment of outliers that predate the onset of the last glaciation in the Uinta Mountains. Such ages can indicate inheritance due to boulder reworking, or that a moraine is a compound feature occupied during MIS 2 and a previous glaciation (e.g., MIS 6, 5d, or 4). In our case, sampling along a single, continuous moraine ridge in each valley minimized the issue of sampling compound moraines, suggesting that boulder reworking is the most likely cause of inheritance. We use the radiocarbon-limited onset of the last glaciation in the Bear River valley, 26 cal. ka (Rosenbaum and Heil, in press), as the cutoff for identifying cosmogenic-exposure ages that indicate inherited nuclides. This issue is further discussed below in Sections 3.2 and 3.7.

We have also eliminated some exposure ages with unacceptably large uncertainties (greater than 10% of the age itself). These large uncertainties may be due to loss of beryllium during the chemical processing of these samples. Since these losses may have fractionated the isotopes of beryllium in the sample, we regard ages with large uncertainties as untrustworthy.

We assign uncertainties to our estimates of moraine age in different ways, depending on the estimator we use to determine

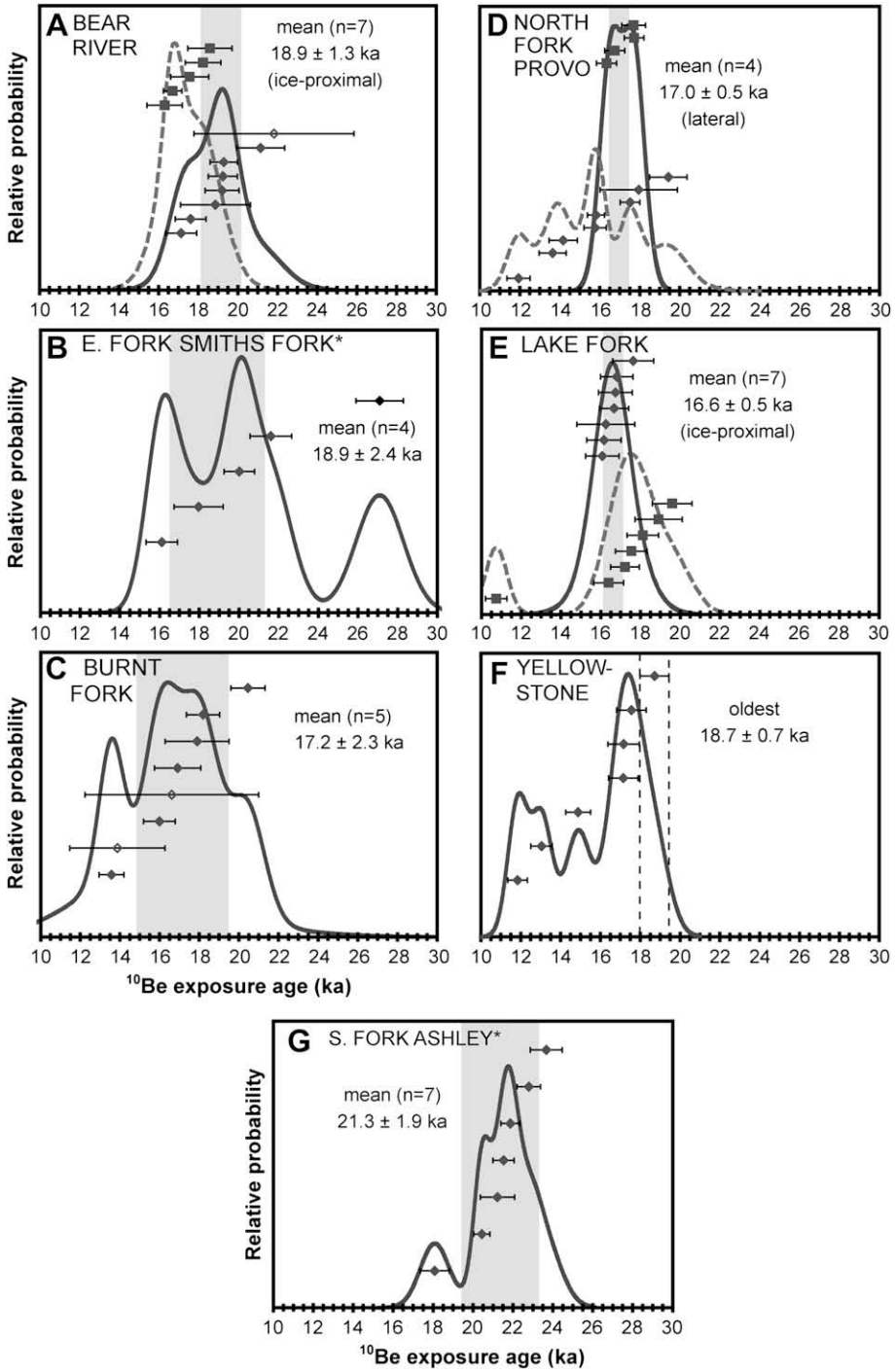

Fig. 6. Probability-density plots of cosmogenic-exposure ages for individual moraines in the Uinta Mountains. On each graph, all plotted samples were used to calculate relative probability; open symbols indicate ages not used for calculating the mean cosmogenic-exposure age. Dashed curves represent the distribution of exposure ages on the ice-distal moraine in the Bear River valley (panel A), the end moraine in the North Fork Provo Valley (panel D), and the ice-distal moraine in the Lake Fork valley (panel E), none of which are used to estimate the time of moraine abandonment in these three valleys. We select either the mean age $\pm 1\sigma$ (gray boxes) or the oldest age (dashed boxes) that is less than 26 cal. ka according to the criteria described in the text (see Section 3). Individual ages (diamonds, $\pm 1\sigma$ uncertainty of AMS analysis) are arranged on each graph from youngest to oldest but are not plotted against relative probability on the vertical axis. Asterisk indicates moraines that yielded cosmogenic-exposure ages predating MIS 2 but are assumed to indicate the presence of inherited nuclides and are not shown here.

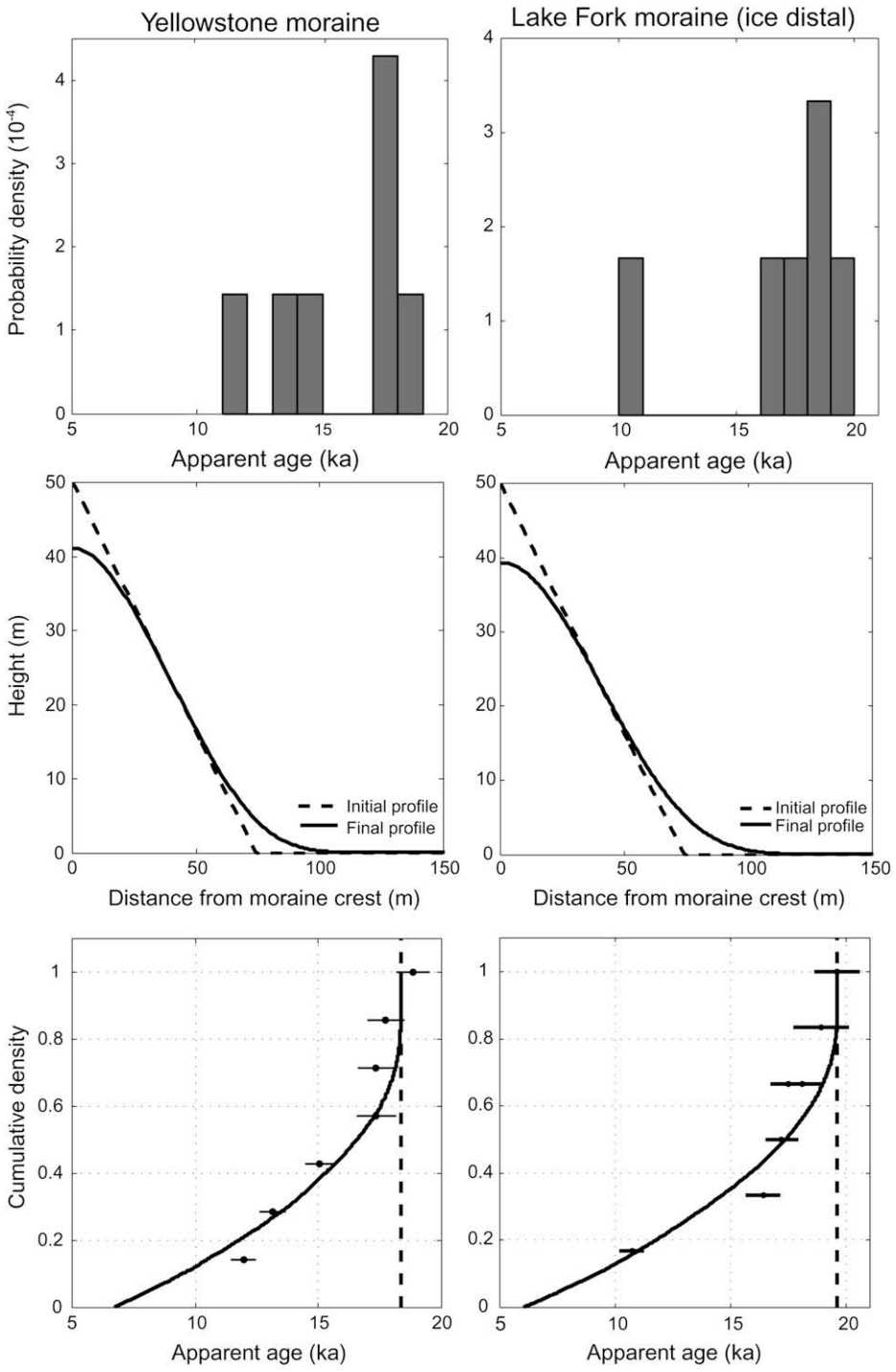

Fig. 7. Histograms of cosmogenic-exposure ages from the Yellowstone moraine and Lake Fork ice-distal moraine (top) and output of a moraine degradation and cosmogenic-nuclide accumulation model (B and C; Applegate et al., 2008). For each moraine, the histograms display several young outliers, which model experiments suggest are consistent with moraine degradation. The evolution of each moraine's profile over 18.5 yr by diffusive hill-slope processes is displayed in the two middle panels. The model runs assume an initial height of 50 m, an initial slope of 34°, and a diffusivity of 7.5×10^{-2} m^2 yr^{-1}. Cosmogenic-exposure ages from the two moraines are plotted in the lower panels (dots and 1σ error bars) along with a distribution of ages predicted by the moraine degradation model for the same model run as shown in the middle panels. For both moraines, the modeled distribution passes within 1σ of all the ages but one. The vertical dashed line in the lower panels shows the assumed true age of the moraines; 18.5 ka for the Yellowstone moraine and 19.6 ka for the Lake Fork moraine. Since this line falls close to the oldest boulder, we take the exposure date yielded by this sample as the best estimator of the age of these two moraines.

the true age of the moraine. Where we use the oldest exposure age, we take the uncertainty to be the 1σ analytical uncertainty of the oldest exposure age. Where we instead used the mean, we assign an uncertainty equal to the standard deviation of the exposure ages. This method of assigning uncertainties accounts for our degree of confidence in our understanding of the geomorphology of each field site. In the two cases where we are reasonably sure about the geomorphic process responsible for the observed scatter, the uncertainties are generally smaller than those of our other age estimates.

We emphasize that this method of selecting the best estimator of moraine age is preliminary. In particular, the best-fit model curves shown in Fig. 7 have been determined by eye, rather than using an objective fitting criterion. We are working to identify an objective fitting criterion to use in producing further model fits. In the future, we plan to use the best-fit moraine age from model results to estimate moraine ages.

The following sections describe results of cosmogenic-exposure dating for seven valleys in the Uinta Mountains in clockwise order, beginning with the Bear River valley (Fig. 1).

3.1. The Bear River valley

Two areas on the terminal-moraine complex in this valley were dated by Laabs et al. (2007a; Fig. 4A). Six cosmogenic-exposure ages from a low-relief, gently rounded ridge on the ice-proximal side of the moraine yield an error-weighted mean of 18.9 ± 1.3 ka. Five ages from a broad, ice-distal area of the moraine that displays high-relief, hummocky topography have a mean of 17.5 ± 1.0 ka (Table 1, Figs. 5 and 6). These two ages overlap at 1σ, but morpho-stratigraphic relations between the two areas of the moraine indicate that their mean ages are reversed. Laabs et al. (2007a) discuss several possible explanations for this result, including a greater degree of degradation of the ice-distal side of the moraine. However, given the relatively small number of cosmogenic-exposure ages on the ice-distal side of the moraine and differing morphologies of the two sampling areas (see Laabs et al., 2007a), evaluating the validity of this explanation is difficult. Following the interpretative approach presented here, we suggest that final ice retreat from the terminal moraine in the Bear River valley began at 18.9 ± 1.3 ka, the mean of cosmogenic-exposure ages from the ice-proximal area of the moraine.

3.2. The East Fork Smiths Fork valley

This area of the northern Uinta Mountains is the type locality for the Pinedale-equivalent Smiths Fork Glaciation (Bradley, 1936). Excellent preservation of a single, sharp-crested moraine loop with abundant tall boulders at the crest was encouraging for cosmogenic-exposure dating in this valley (Fig. 4B); however, the resulting data set is difficult to interpret unequivocally due to broad scatter of cosmogenic-exposure ages from the moraine. Nine cosmogenic-exposure ages from this moraine range from 16.1 ± 1.6 ka to 51.9 ± 7.6 ka (1σ, Table 1, Figs. 5 and 6), with five ages predating MIS 2 and four falling within this time interval. After eliminating ages with very high analytical error (see explanation in Table 1), three of seven ages predate MIS 2. When considered alone, the distribution of ages precludes accurate determination of whether exposure ages that predate MIS 2 reflect inherited nuclides due to reworking, if this moraine was deposited during a previous glaciation, or if the moraine is a compound feature. However, two of the three boulders that yield pre-MIS 2 ages are in ice-proximal positions at the moraine crest relative to two of the four boulders that yield ages within the interval MIS 2. If the moraine were a compound feature occupied during MIS 4 and MIS 2, we would expect to find boulders with older exposure ages on the distal part of the moraine crest. The observed pattern therefore suggests that pre-MIS 2 exposure ages are due to inherited nuclides, consistent with our glacial mapping and that of Bradley (1936). The cosmogenic-exposure age of sample EFSF-10 (27.1 ± 1.2 ka) narrowly overlaps the estimate for the onset of the Smiths Fork Glaciation (26 cal. ka), but likely does not represent the time of moraine abandonment. We consider the mean of the remaining four ages to represent the time of moraine abandonment, at 18.9 ± 2.4 ka.

3.3. The Burnt Fork valley

In this valley, we sampled two sharp-crested lateral moraines in this valley that grade to a well-preserved terminal moraine (Fig. 4C). Both sampled moraines are more than 4 km in length and have as much as 60 m of relief. We sampled the lateral moraines because they are more continuous and contained more boulders suitable for cosmogenic-exposure dating than any section of the terminal moraine, and both clearly grade to the moraine indicating that they were deposited at the same time. Eight cosmogenic-exposure ages on the lateral moraine range from 13.6 ± 0.6 ka to 20.5 ± 0.9 ka (1σ; Table 1, Figs. 5 and 6), forming a nearly symmetrical distribution of ages with a mean of 17.2 ± 2.3 ka. Although the broad range of ages on this moraine may be suggestive of some moraine degradation, the distribution of ages suggests that the mean is a better estimate of the time of moraine abandonment than the oldest exposure age.

3.4. The South Fork Ashley Creek valley

The head of this valley was occupied by the easternmost glacier in the Uinta Mountains during the last glaciation. The glacier was relatively small ($\sim$18 km in length compared to 30–40 km in other valleys reported in this study), but preservation of a broad, hummocky moraine is excellent (Fig. 4D). We sampled boulders on a continuous moraine loop at the distal edge of the moraine to avoid issues of boulder exhumation due to differential melting of buried ice in the area of hummocky topography. These boulders yield cosmogenic-exposure ages ranging from 18.0 ± 1.5 ka to 56.1 ± 3.5 ka (1σ, Table 1, Figs. 5 and 6). Here, three of ten sampled boulders yield pre-MIS 2 exposure ages, suggesting that the moraine is a compound feature or that boulders contain significant inherited nuclides. Because all of the boulders were collected from the same, narrow-crested continuous ridge, we favor the latter explanation. The seven remaining cosmogenic-exposure ages are distributed symmetrically about a mean age of 21.3 ± 1.9 ka, suggesting that ice began retreating from the distal part of the terminal moraine at this time.

3.5. The Yellowstone River valley

The glacier terminus in this valley was very near the glacier terminus in the Lake Fork valley (Figs. 1, 4E) and is marked by an extensive terminal-moraine complex near the mouth of the Yellowstone canyon (Laabs, 2004; Munroe et al., 2006). Much of the terminal moraine is on private land and was inaccessible for this study, yet seven cosmogenic-exposure ages of moraine boulders on a narrow, sharp-crested left-lateral moraine, which clearly is a continuation of the terminal moraine, range from 11.8 ± 0.5 ka to 18.7 ± 0.7 ka (1σ; Table 1, Figs. 5 and 6). As noted above, the left-skewed distribution of these ages suggests that the oldest age best approximates the time of moraine abandonment, at 18.7 ± 0.7 ka.

3.6. The Lake Fork valley

One of the best preserved moraine sequences in the Uinta Mountains is found near the mouth of the Lake Fork canyon (Munroe et al., 2006; Fig. 4E). Laabs (2004) sampled ice-distal and ice-proximal ridges on this moraine, both of which form narrow, sharp-crested right-lateral ridges that become frontal ridges near the center of the valley. Seven boulders on the ice-distal ridge yield cosmogenic-exposure ages ranging from 10.7 ± 0.5 ka to 19.6 ± 1.0 ka (1σ, Table 1, Figs. 5 and 6). The distribution of ages from this part of the moraine is left skewed, suggesting that the oldest age best approximates the time of moraine abandonment, at 19.6 ± 1.0 ka. Seven cosmogenic-exposure ages from the ice-proximal ridge have a mean age of 16.6 ± 0.5 ka, suggesting that glacier ice in the Lake Fork valley persisted at the terminal moraine until this time or readvanced to its Smiths Fork maximum at this time.

3.7. The North Fork Provo River valley

A well-preserved sequence of lateral and end moraines from the Smiths Fork Glaciation exists near the confluence of the North Fork and Provo Rivers (Fig. 4F). Refsnider et al. (2008) sampled an area within the sequence in which a sharp-crested left-lateral moraine becomes a relatively broad end moraine with hummocky topography at its crest. Eight samples from the end moraine yield cosmogenic-exposure ages ranging from 11.9 ± 0.6 ka to 19.4 ± 0.9 ka, and four samples from the lateral moraine (about 1 km up-valley from the end moraine) yield ages ranging from 16.3 ± 0.5 ka to 17.7 ± 0.6 ka (1σ, Table 1, Figs. 5 and 6). Ages on the end moraine display broad scatter but, unlike other moraines with similar scatter, are uniformly distributed about a mean age of 15.8 ± 2.5 ka. In this case, the lack of overlap (at the 1σ level) raises question to whether (1) the scatter reflects relatively large systematic errors due to boulder shielding and inheritance, (2) the moraine crest degraded rapidly at times indicated by individual exposure ages, or (3) the ice margin fluctuated at its terminal moraine and added boulders to it for several millennia. The moraine does not bear characteristics of a compound feature, and the close proximity of the sample sites (Fig. 4F) suggests that differential erosion cannot explain the scatter of ages. However, the mean of cosmogenic-exposure ages from the terminal moraine overlaps with all four ages from the lateral moraine, which range narrowly about a mean age of 17.1 ± 0.7 ka. If the four boulders on the lateral moraine were indeed deposited just prior to moraine abandonment and have not been exhumed, then ice in the North Fork Provo River valley was still near its Smiths Fork maximum extent at about 17.1 ± 0.7 ka.

4. Discussion

4.1. Cosmogenic-exposure age variability in the Uinta Mountains – climatic and non-climatic explanations

As noted above, one advantage of obtaining cosmogenic-exposure ages from multiple valleys within the Uinta Mountains is that spatial differences in the *in situ* production rate of ^{10}Be are minimal. Therefore, the variability of cosmogenic ^{10}Be exposure ages of moraine boulders throughout the Uinta Mountains is chiefly due to either (1) differences in the relative timing of moraine abandonment among the studied valleys, or (2) differences in exposure histories of moraine boulders resulting from post-depositional geologic phenomena (e.g., erosion-induced exhumation of boulders, shielding from cosmic radiation by snow, etc.), or (3) a combination of these. Although our boulder-sampling strategy and approach to interpreting cosmogenic-exposure ages aim to overcome potential geologic uncertainties of age estimates, we cannot rule out the possibility that geologic factors have influenced the variability of our cosmogenic-exposure ages.

In the following discussion, we assume that our age estimates for terminal-moraine abandonment in each valley (described above) are accurate, and that variability among these ages is due to local differences in climate within the Uinta Mountains. We then highlight the potential issues raised by this assumption and identify areas where additional data are needed to develop a more precise chronology of glaciation in the range.

4.1.1. Climatic explanations

The oldest age estimate of terminal-moraine abandonment (i.e., the start of ice retreat) in the Uinta Mountains is in the easternmost glacial valley in the range. Ice retreat began at 21.3 ± 1.9 ka in the South Fork Ashley Creek valley. In contrast, glaciers persisted at or near their maximum extents until as much as ~4 kyr later in southern and western valleys: the latest age estimates for the start of ice retreat in this part of the range are 17.1 ± 0.7 ka in the North Fork Provo valley and 16.6 ± 0.5 ka in the Lake Fork valley (Fig. 1 and 5). A later start of overall ice retreat in the southwestern Uinta Mountains is consistent with the hypothesis that Lake Bonneville influenced glacier mass balance at the upwind end of the range (McCoy and Williams, 1985; Munroe and Mickelson, 2002), where glacier ELAs were lowest, while the lake remained at or above the Provo shoreline until about 16 ka (Oviatt, 1997) or possibly later (Godsey et al., 2005). Furthermore, the subsequent start of ice retreat in southwestern valleys was approximately synchronous with the fall of Lake Bonneville, suggesting that the lake and glaciers in these valleys responded to the same regional-scale climate changes.

The early start of ice retreat in the Bear River valley (18.9 ± 1.3 ka) relative to other valleys at the upwind end of the range appears inconsistent with this theory, but may reflect slight differences in north–south atmospheric circulation or differences in ice-response times among the valleys. For example, Laabs et al. (2007a) note that southwest to northeast circulation across the Great Basin to the Uinta Mountains may have left the northern slope of the range in an orographic precipitation-shadow. This could explain the slightly older age estimates for moraine abandonment in the Bear River valley relative to the North Fork Provo and Lake Fork valleys. Supporting evidence for this hypothesis includes the relatively broad surface area of glacier ice in southwestern valleys compared to northwestern valleys (Fig. 1). Additionally, recent mapping by Munroe and Laabs (in press) documents significant latest Pleistocene ice cover (more than 71 km^2) in the extreme southwestern part of the Uinta Mountains region (Fig. 1) with terminus and cirque-headwall elevations (2000 and 3000 m asl, respectively) as much as 1000 m lower than elsewhere in the range. In contrast, evidence for glaciation at such low elevations in the northwestern Uinta Mountains has not been observed. An alternative explanation is that the ice field draining into the Bear River and North Fork Provo valleys may have responded more slowly (and perhaps asymmetrically) to changes in climate than the smaller, discrete, valley glacier in the Lake Fork valley.

4.1.2. Non-climatic explanations

Although we are confident in our interpretations of the cosmogenic ^{10}Be surface-exposure ages reported here, it is worth exploring the potential non-climatic explanations of variability of cosmogenic-exposure ages in the Uinta Mountains that may be related to difficulty in accurately interpreting some data sets. For instance, our estimate for the time when the terminal moraine in the East Fork Smiths Fork valley was abandoned is based on

a widely scattered distribution of only four ages, from which we have selected the mean of cosmogenic-exposure ages that post date the onset of glaciation in the Bear River valley at 26 cal. ka. Additional boulder sampling here might aid in setting more precise limits on the age of latest Pleistocene moraine abandonment, and may clarify whether boulders with relatively old cosmogenic-exposure ages have been reworked or if the terminal moraine in the Smiths Fork valley is actually a compound feature formed by multiple glacial advances. As noted above, however, detailed mapping and careful sampling of these moraines (Munroe and Laabs, in press) indicate that we sampled boulders from a single, distal terminal-moraine crest (Fig. 4).

Additionally, our ability to obtain a relatively young cosmogenic-exposure age of the ice-proximal ridge of the Lake Fork terminal moraine may be due in part to the excellent preservation of this moraine complex and the abundance of boulders suitable for cosmogenic-exposure dating. Multi-crested terminal-moraine complexes are present in several other valleys we sampled in the range, but in all valleys except the Lake Fork and Bear River our sampling was limited to the most prominent, ice-distal ridge. Therefore, it is possible that the less well-developed ice-proximal or recessional moraine ridges in other valleys, including those in the Bear River and East Fork Smiths Fork valleys, may have formed as late as 16 ka, similar to that dated in the Lake Fork. However, these moraines generally lack boulders suitable for cosmogenic-exposure dating and our sampling strategy favored moraines with abundant boulders to minimize geologic uncertainties of cosmogenic-exposure dating and to reduce statistical uncertainties of mean ages. Dating of small numbers (1–4) of boulders from ice-proximal and recessional moraine ridges in these valleys might provide further age limits for the start of terminal deglaciation, although data sets of such size can be difficult to interpret.

Despite these potential alternative interpretations, it is worth noting that even if the undated ice-proximal or recessional moraines in other valleys were deposited as late as 16 ka, such moraines are not present in all valleys. For instance, the absence of recessional moraines in the South Fork Ashley Creek drainage suggests that rapid and monotonic ice retreat there began at the time indicated by the cosmogenic-exposure ages on the terminal moraine, 21.3 ± 1.9 ka. Thus, the range-wide set of ages reported here still indicates a significant age disparity in the start of ice retreat in southern and western valleys relative to this easternmost valley (if not all dated northern *and* eastern) valleys in the Uinta Mountains (Fig. 6e–g).

Furthermore, consideration of all cosmogenic-exposure ages from the Uinta Mountains indicates that age disparities between northern and eastern valleys and southern and western valleys are not an artifact of our interpretive model. The probability-density plots shown in Fig. 8 reveal that the maximum probability of all ages falling within the interval MIS 2 from northern and eastern valleys is ~22–20 ka ($n = 20$), whereas this range is ~18–16.5 ka for southern and western valleys ($n = 44$). This pattern is due primarily to the large number of samples with exposure ages greater than 20 ka from the South Fork of Ashley Creek and the large number of samples from the Lake Fork, Yellowstone, and North Fork Provo valleys with exposure ages within the range 18–16.5 ka. As shown in Fig. 5, applying the "oldest boulder" method of interpreting cosmogenic-exposure ages to all moraines would still lead to the conclusion that ice retreat in the South Fork Ashley Creek valley began as much as ~4 kyr prior to retreat from the ice-proximal moraine in the Lake Fork and the terminal moraine the North Fork Provo valley (Fig. 5). Based on these observations, and the dramatic west-to-east rise in glacier ELAs across the Uinta Mountains during the last glaciation (Munroe and Mickelson, 2002), we favor the interpretation that differences in cosmogenic-exposure ages indicate range-scale variability in the time of ice retreat driven by climatic forces (see Section 4.1.1).

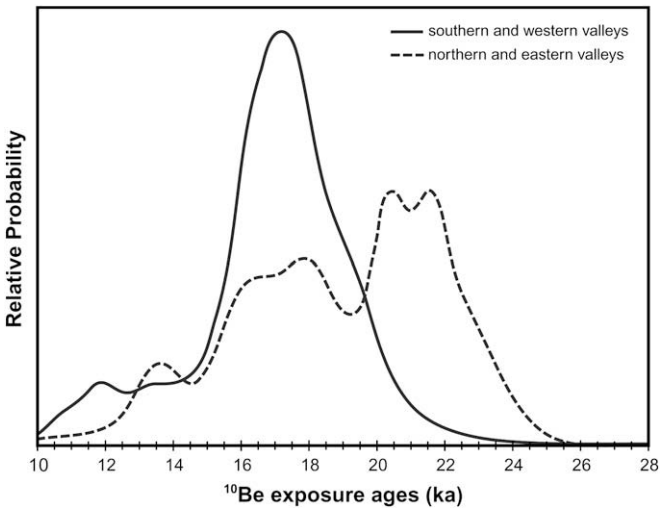

Fig. 8. Probability-density plots of all cosmogenic-exposure ages within the interval MIS 2 from the Smiths Fork, Burnt Fork, and South Fork Ashley Creek valleys (dashed curve) of the northern and eastern Uinta Mountains where ELAs of the Smiths Fork Glaciation were 3100–3200 m asl, and of all cosmogenic-exposure ages in the Bear River, North Fork Provo, Lake Fork, and Yellowstone valleys (solid curve) of the western and southern Uinta Mountains where ELAs were as much as 400 m lower (2800–3000 m asl).

4.2. Cosmogenic-exposure age limits on moraine abandonment in the Great Basin/Rocky Mountains region and paleoclimatic inferences

Despite the potential influence of non-climatic factors on the variability of cosmogenic-exposure ages, the age estimates for moraine abandonment in the Uinta Mountains reported here are meaningful and suggestive of spatial differences in the timing of ice retreat, at least until more data are available. Next, we place cosmogenic-exposure age estimates from the Uinta Mountains into a regional context by comparing them with ages from elsewhere in the Rocky Mountains. For this purpose, all cosmogenic ^{10}Be exposure ages listed below from outside the Uinta Mountains have been recalculated using the production rate and scaling scheme described in Balco et al. (2008).

The onset of glaciation in the Bear River valley at 26 cal. ka (Rosenbaum and Heil, in press) is consistent with radiocarbon-age limits on glacial sediment preserved in lakes of the Colorado Front Range (Nelson et al., 1979). Ice retreat in the southwestern Uinta Mountains at 18–16.5 ka was approximately synchronous with, or slightly later than, retreat in the northern Rocky Mountains (see dated locales in Fig. 3). In this region, outlets of the Yellowstone ice cap began retreating at about 18.8–16.5 ka (based on ^{10}Be and ^{3}He cosmogenic-exposure dating, Licciardi et al., 2001; Licciardi and Pierce, 2008), and a valley glacier in the Wallowa Mountains (northeastern Oregon) began retreating at 17.2 ± 0.8 ka (1σ, based on ^{10}Be cosmogenic-exposure dating; Licciardi et al., 2004). A radiocarbon-based glacial chronology indicates that valley glaciers in the Sawtooth Range, in southern Idaho, also began retreating at this time, after about 16.9 ± 0.4 cal. ka (Thackray et al., 2004).

As noted above, the approximate synchrony of ice retreat in the southern and western Uinta Mountains and the hydrologic fall of Lake Bonneville from the Provo shoreline at about 16 ka suggest that glaciers and Lake Bonneville sustained their maxima until 4–5 kyr after the global LGM (21 ± 2 cal. ka, or possibly earlier; Peltier and Fairbanks, 2006). The late highstand of Lake Bonneville

relative to the time of the global LGM has been attributed to increased effective precipitation accompanying migration of the polar jet and associated storm tracks northward following the retreating margin of the Laurentide Ice Sheet (Benson and Thompson, 1987; Bartlein et al., 1998). Although further development of latest Pleistocene glacier and pluvial lake chronologies is necessary to test this hypothesis, recently developed lake-level chronologies for the extreme southwestern U.S. indicate pluvial lake expansion in southern New Mexico and west Texas (e.g., Wilkins and Currey, 1997; Krider, 1998) prior to and during the global LGM and therefore prior to the expansion of Lake Bonneville. Licciardi et al. (2004) and Thackray et al. (2004) have also attributed the relatively late maxima of glaciers in the northern Rocky Mountains to increased moisture availability after 21 ka induced by retreat of North American ice sheets. Thus, there is growing evidence that precipitation controls on glacier mass balance were significant and that regional-scale climate change was important in determining the timing of the start of ice retreat in the Uinta Mountains and other ranges of the Rocky Mountains.

If the presence of Lake Bonneville significantly impacted glacier mass balance in the southern and western valleys of the Uinta Mountains, thereby sustaining glacier maxima there later than in the northern and eastern valleys, it may have done so in a variety of ways. For example, reduced glacier ablation may have been caused by decreased melt-season temperatures or increased cloudiness in adjacent areas, similar to effects seen near the modern Great Lakes (Changnon and Jones, 1972). In addition, the presence of a large lake in the Bonneville basin may have induced "lake-effect" precipitation, enhancing snow accumulation in areas downwind of the lake (Zielinski and McCoy, 1987), including the Wasatch and Uinta Mountains. In addition to the 400-m, west-to-east rise in glacier ELAs across the Uinta Mountains (Munroe and Mickelson, 2002), this potential impact is supported by several observations: first, modern winter precipitation patterns in the Wasatch and Uinta Mountains (Fig. 2; PRISM reconstruction, http://www.prism.oregonstate.edu) reveal that the southwestern Uinta Mountains receive almost the same amount of precipitation as the western Wasatch Mountains, indicating that although the Wasatch Mountains are a clear topographic barrier, they do not induce a precipitation-shadow on the leeward Uinta Mountains. Second, the Great Salt Lake – which has a surface area of about one-tenth that of Lake Bonneville – provides winter lake effect precipitation that falls in the Wasatch and western Uinta Mountains (Carpenter, 1993), also suggesting substantial west-to-east moisture advection across the Wasatch Mountains. Third, numerical modeling of regional-scale atmospheric circulation and lake-atmosphere feedbacks during the Lake Bonneville highstand shows that the presence of the lake had a greater impact on precipitation than on temperature in adjacent regions (Hostetler et al., 1994). Finally, region-wide glacier reconstructions (Leonard, 2007) and numerical glacier modeling experiments (McCoy and Williams, 1985; Laabs et al., 2006; Refsnider et al., 2008) show that LGM ice extents in the Wasatch and western Uinta Mountains can be simulated only by greater-than-modern precipitation even with temperature depressions of 6–9 °C. Thus, we suggest that glaciers in the southern and western Uinta Mountains persisted at or near their maxima later than those in eastern valleys because they were closer to Lake Bonneville, a local source of significant moisture.

Although this and other recently developed glacial chronologies for the Rocky Mountains are suggestive of significant precipitation controls on ice extent near the end of the local LGM, some paleoclimatic studies characterize the local LGM as very cold, as much as 15 °C colder than modern, and relatively dry in this region (e.g., Porter et al., 1983; Murray and Locke, 1989). Perhaps the most robust, quantitative estimates of paleotemperature during the local LGM are from Kaufman (2003), who estimates a temperature depression of 7–13 °C from 24 to 12 cal. ka based on radiocarbon dating and amino-acid paleothermometry of fossil mollusks in deposits of Lake Bonneville. Numerical glacier modeling experiments in the Wasatch and western Uinta Mountains (Laabs et al., 2006; Refsnider et al., 2008) suggest that temperature depressions of more than 9 °C would have been accompanied by less-than-modern precipitation in this area. However, it is unclear whether the paleotemperature estimates of Kaufman (2003) reflect uniform depression of mean-annual temperature, or perhaps greater depressions of summer temperature that could reduce evapotranspiration over Lake Bonneville and glacier melting in neighboring mountain ranges. Therefore, more precise limits on temperature and precipitation in this region near the end of the local LGM are needed. We favor the explanation that the relatively large temperature depressions estimated by Kaufman (2003) persisted during the global LGM while the southern branch of the polar jet was located south of the Lake Bonneville basin. Subsequent retreat of North American ice sheets and the accompanying northward shift of the jet resulted in increased precipitation, allowing Lake Bonneville to rise and glaciers to persist at or readvance to their maximum extents in the southwestern Uinta Mountains until about 16 ka.

The start of ice retreat at 22–20 ka in the northern and eastern glacial valleys of the Uintas was approximately synchronous with that in the central Colorado Plateau and in the Middle Rocky Mountains of Colorado and Wyoming. Marchetti et al. (2005) report a set of cosmogenic ^{3}He exposure ages of terminal moraines near Boulder Mountain (Utah) that range from 23.1 ± 1.3 ka to 20.0 ± 1.4 ka. Gosse et al. (1995) report several cosmogenic ^{10}Be exposure ages from terminal moraines in the Wind River Mountains; the average of these ages is 21.0 ka. The oldest cosmogenic-exposure age from the youngest recessional moraine dated by Gosse et al. (1995) is 19.1 ± 1.1 ka, suggesting that ice retreat was underway by this time. In Colorado, Benson et al. (2005) document cosmogenic ^{36}Cl exposure ages of moraine boulders with mean ages of 18.4 ka in north-central mountain ranges and of 18.9 ka in the San Juan Mountains (southwestern Colorado). In central Colorado, Brugger (2007) report cosmogenic ^{10}Be exposure ages of terminal moraines that range from 21.4 ± 1.7 to 16.5 ± 2.1 ka, and Guido et al. (2007) find that ice retreat in the Animas River valley (San Juan Mountains, southwestern Colorado) was underway by 19.4 ± 1.5 ka. The cause of ice retreat in the northern and eastern Uinta Mountains and elsewhere in the western U.S. during or near the end of the global LGM ($\sim$21 ka) is difficult to identify. As suggested by Licciardi et al. (2004), glaciers in northern ranges may have become moisture starved due to the presence of the Laurentide ice sheet, or the regional-scale warming of the North Atlantic region at this time may have had far-reaching effects in the western U.S.

5. Summary

Based on 74 cosmogenic ^{10}Be surface-exposure ages, the last glaciation in the Uinta Mountains (the Smiths Fork Glaciation) culminated during MIS 2. Radiocarbon-age limits on glacially derived lacustrine sediment in Bear Lake (beyond the glacial limit in the Bear River drainage) suggest the onset of glaciation occurred at 26 cal. ka and that the Smiths Fork Glacial Maximum occurred by 20 cal. ka (Rosenbaum and Heil, in press). If our interpretations of cosmogenic-exposure ages of moraine boulders in seven valleys are accurate, then the start of deglaciation in the Uinta Mountains occurred at about 22–20 ka in northern and eastern valleys, and at 18–16.5 ka in southern and western valleys. Glaciers in the northern and eastern Uinta Mountains began retreating in phase

with glaciers in the Wind River Range to the north and with glaciers in other locations to the east and southeast. The start of ice retreat in western and southern valleys of the Uinta Mountains was delayed until after the global LGM and was approximately synchronous with that in the northern Rocky Mountains and with the hydrologic fall of Lake Bonneville from the Provo shoreline. As noted by Licciardi et al. (2004) and Thackray et al. (2004), regional-scale variability in the timing of deglaciation could reflect differences in the availability of moisture. Within the Uinta Mountains, glaciers nearest to Lake Bonneville persisted at or readvanced to their maxima at 16 ka due to enhanced precipitation driven by northward migration of the polar jet and associated storm tracks (e.g., Benson and Thompson, 1987), amplified by a pluvial lake effect (Munroe and Mickelson, 2002; Munroe et al., 2006). In contrast, glaciers located farther from the lake retreated earlier, although the cause of their retreat is unclear.

Despite the range-wide approach to cosmogenic-exposure dating of moraines described here, challenges of interpreting cosmogenic-exposure age distributions from moraines somewhat limit our ability to infer the latest Pleistocene glacial history of the Uinta Mountains. Additional cosmogenic-exposure dating of ice-proximal and recessional moraines in these mountains further development of the glacial chronology in the Wasatch Mountains (e.g., Laabs et al., 2007b), and more precise limits on latest Pleistocene temperatures in the region would further improve this chronology and support the development of more sophisticated paleoclimate reconstructions.

Acknowledgments

This project was funded by NSF/EAR- 0345277 and NSF/EAR-0345112 and by support from the Purdue University PRIME Lab. We thank Olena Krawciw, Kate Lawson, Andy Rishavy, Chris Rodgers, Colin Rodgers, Jeremy Shakun, Jesse Silverman, and Tom Westlund for assistance in the field. We thank Richard Becker, Daniel Douglass, Shasta Marrero, Brad Sleeth, and Liubing Xu for assistance in the lab. Reviews by J. Licciardi and an anonymous reviewer were very helpful in developing this paper.

References

Applegate, P.J., Lowell, T.V., Alley, R.B., 2008. Comment on "Absence of cooling in New Zealand and the adjacent ocean during the younger Dryas Chronozone". Science 320, 746d.

Atwood, W.W., 1909. Glaciation of the Uinta and Wasatch Mountains. U.S. Geological Survey Professional Paper 61 96pp.

Balco, G., Schaefer, J.M., 2006. Cosmogenic-nuclide and varve chronologies for the deglaciation of southern New England. Quaternary Geochronology 1, 15–28.

Balco, G., Stone, J.O., Lifton, N.A., Dunai, T.J., 2008. A complete and accessible means of calculating surface exposure ages or erosion rates from ^{10}Be and ^{26}Al measurements. Quaternary Geochronology 3, 174–195.

Bartlein, P.J., Anderson, K.H., Anderson, P.M., Edwards, M.E., Mock, C.J., Thompson, R.S., Webb, R.S., Webb III, T., Whitlock, C., 1998. Paleoclimate simulations for North America over the past 21,000 years: features of the simulated climate and comparisons with paleoenvironmental data. Quaternary Science Reviews 17, 549–585.

Benson, L., Thompson, R.S., 1987. The physical record of lakes in the Great Basin. In: Ruddiman, W.F., Wright Jr., H.E. (Eds.), North American and Adjacent Oceans during the Last Deglaciation, vol. K-3. Geological Society of America, The Geology of North America, Boulder, CO, pp. 241–260.

Benson, L., Madole, R., Landis, G., Gosse, J., 2005. New data for late Pleistocene Pinedale alpine glaciation from southwestern Colorado. Quaternary Science Reviews 24, 49–65.

Bevington, P.R., Robinson, D.K., 2002. Data Reduction and Error Analysis for the Physical Sciences. McGraw-Hill High Education, 336 pp.

Bierman, P.R., Caffee, M.W., Davis, P.T., Marsella, K., Pavich, M., Colgan, P., Mickelson, D., Larsen, J., 2002. Rates and timing of Earth-surface processes from in situ-produced cosmogenic Be-10. In: Grew, E.S. (Ed.), Beryllium – Mineralogy, Petrology and Geochemistry. Reviews in Mineralogy and Geochemistry, vol. 50. Mineralogical Society of America and Geochemical Society, Washington D.C., pp. 147–205.

Bradley, W.A., 1936. Geomorphology of the north flank of the Uinta Mountains. U.S. Geological Survey Professional Paper 185-I, 163–169.

Briner, J.P., Kaufman, D.S., Manley, W.F., Finkel, R.C., Caffee, M.W., 2005. Cosmogenic exposure dating of late Pleistocene moraine stabilization in Alaska. Geological Society of America Bulletin 117 (7/8), 1108–1120.

Brugger, K.A., 2007. Cosmogenic ^{10}Be and ^{36}Cl ages from Late Pleistocene terminal moraine complexes in the Taylor River drainage basin, central Colorado, USA. Quaternary Science Reviews 26, 494–499.

Bryant, B., 1992. Geologic and structure maps of the Salt Lake City $1^\circ \times 2^\circ$ quadrangle, Utah and Wyoming. U.S. Geological Survey Miscellaneous Investigations Series Map, I-1997: 1:125,000 scale.

Carpenter, D.M., 1993. The lake effect of the Great Salt Lake – overview and forecast problems. Weather and Forecasting 8, 181–193.

Changnon, S.A., Jones, D.M.A., 1972. Review of the influences of the Great Lakes on weather. Water Resources Research 8, 360–371.

Desilets, D., Zreda, M., 2001. On scaling cosmogenic nuclide production rates for altitude and latitude using cosmic-ray measurements. Earth and Planetary Science Letters 193, 197–212.

Gillespie, A., Molnar, P., 1995. Asynchronous maximum advances of mountain and continental glaciers. Reviews of Geophysics 33, 311–364.

Godsey, H.S., Currey, D.R., Chan, M.A., 2005. New evidence for an extended occupation of the Provo shoreline and implications for regional climate change, Pleistocene Lake Bonneville, Utah, USA. Quaternary Research 63, 212–223.

Gosse, J.C., Phillips, F.M., 2001. Terrestrial in situ cosmogenic nuclides: theory and application. Quaternary Science Reviews 20, 1475–1560.

Gosse, J.C., Klein, J., Evenson, E.B., Lawn, B., Middleton, R., 1995. Beryllium-10 dating of the duration and retreat of the last Pinedale glacial sequence. Science 268, 1329–1333.

Granger, D.E., Muzikar, P.F., 2001. Dating sediment burial with in situ-produced cosmogenic nuclides: Theory, techniques, and limitations. Earth and Planetary Science Letters 188, 269–281.

Guido, Z.S., Ward, D.J., Anderson, R.S., 2007. Pacing the post-Last Glacial Maximum demise of the Animas Valley glacier and the San Juan Mountain ice cap, Colorado. Geology 35, 739–742.

Hallet, B., Putkonen, J., 1994. Surface dating of dynamic landforms: young boulders on aging moraines. Science 265 (5174), 937–940.

Heisinger, B., Lal, D., Jull, A.J.T., Kubik, P.W., Ivy-Ochs, S., Neumaier, S., Knie, K., Lazarev, V., Nolte, E., 2002a. Production of selected cosmogenic radionuclides by muons: 1. Fast muons. Earth and Planetary Science Letters 200, 345–355.

Heisinger, B., Lal, D., Jull, A.J.T., Kubik, P.W., Ivy-Ochs, S., Knie, K., Nolte, E., 2002b. Production of selected cosmogenic radionuclides by muons: 2. Capture of negative muons. Earth and Planetary Science Letters 200, 357–369.

Hostetler, S.W., Giorgi, F., Bates, G.T., Bartlein, P.J., 1994. Lake-atmosphere feedbacks associated with paleolakes Bonneville and Lahontan. Science 263, 665–668.

Imbrie, J., Hays, J.D., Martinson, D.G., McIntyre, A., Mix, A.C., Morley, J.J., Pisias, N.G., Prell, W.L., Shackleton, N.J., 1984. The orbital theory of Pleistocene climate: support from a revised chronology of the marine ^{18}O record. In: Berger, A., Imbrie, J., Hays, J., Kukla, G., Saltzman, B. (Eds.), Milankovitch and Climate Part I. Reidel, Dordrecht, Holland, pp. 269–306.

Ivy-Ochs, S., Kerschner, H., Schlüchter, C., 2007. Cosmogenic nuclides and the dating of Lateglacial and Early Holocene glacier variations: the Alpine perspective. Quaternary International 164–165, 53–63.

Kaplan, M.R., Douglass, D.C., Singer, B.S., Ackert, R.P., Caffee, M.W., 2005. Cosmogenic nuclide chronology of pre-last glaciation maximum moraines at Lago Buenos Aires, 46°S, Argentina. Quaternary Research 63, 301–315.

Kaufman, D.S., 2003. Amino acid paleothermometry of Quaternary ostracodes from the Bonneville Basin, Utah. Quaternary Science Reviews 22, 899–914.

Krider, P.R., 1998. Paleoclimatic significance of late Quaternary lacustrine and alluvial stratigraphy, Animas Valley, New Mexico. Quaternary Research 50, 283–289.

Laabs, B.J.C., 2004. Late Quaternary glacial and paleoclimate history of the southern Uinta Mountains, Utah. Ph.D. thesis, Madison, University of Wisconsin, 162 pp.

Laabs, B.J.C., Carson, E.C., 2005. Glacial geology of the southern Uinta Mountains. In: Dehler, C.M., Pederson, J.L. (Eds.), Uinta Mountain Geology. Utah Geological Association Publication 33, pp. 235–253.

Laabs, B.J.C., Plummer, M.A., Mickelson, D.M., 2006. Climate during the Last Glacial Maximum in the Wasatch and southern Uinta Mountains inferred from glacier modeling. Geomorphology 75, 300–317.

Laabs, B.J.C., Munroe, J.S., Rosenbaum, J.G., Refsnider, K.A., Mickelson, D.M., Singer, B.S., Caffee, M.W., 2007a. Chronology of the Last Glacial Maximum in the upper Bear River basin, Utah. Arctic, Antarctic and Alpine Research 39 (4), 537–548.

Laabs, B.J.C., Bash, E.B., Refsnider, K.A., Becker, R.A., Munroe, J.M., Mickelson, D.M., Singer, B.S., 2007b. Cosmogenic surface-exposure age limits for latest-Pleistocene glaciation and paleoclimatic inferences in the American Fork Canyon, Wasatch Mountains, Utah, U.S.A. Eos, Transactions of the American Geophysical Union 88 (52), Fall Meeting Supplement, Abstract PP33B-1274.

Lal, D., 1991. Cosmic ray labeling of erosion surfaces: in situ nuclide production rates and erosion rates. Earth and Planetary Science Letters 104, 424–439.

Leonard, E., 2007. Modeled patterns of Late Pleistocene glacier inception and growth in the Southern and Central Rocky Mountains, USA: sensitivity to climate change and paleoclimatic implications. Quaternary Science Reviews 26, 2152–2166.

Licciardi, J.M., Pierce, K.L., 2008. Cosmogenic exposure-age chronologies of Pinedale and Bull Lake glaciations in greater Yellowstone and the Teton Range, USA. Quaternary Science Reviews 27, 814–831.

Licciardi, J.M., Clark, P.U., Brook, E.J., Elmore, D., Sharma, P., 2004. Variable responses of western U.S. glaciers during the last deglaciation. Geology 32, 81–84.
Licciardi, J.M., Clark, P.U., Brook, E.J., Pierce, K.J., Kurz, M.D., Elmore, D., Sharma, P., 2001. Cosmogenic ^{3}He and ^{10}Be chronologies of the late Pinedale northern Yellowstone ice cap, Montana, USA. Geology 29, 1095–1098.
Marchetti, D.W., Cerling, T.E., Lips, E.W., 2005. A glacial chronology for the Fish Creek drainage of Boulder Mountain, USA. Quaternary Research 64, 263–271.
McCoy, W.D., Williams, L.D., 1985. Application of an energy-balance model to the late Pleistocene Little Cottonwood Canyon glacier with implications regarding the paleohydrology of Lake Bonneville. In: Kay, P.A., Diaz, H.F. (Eds.), Problems of and Prospects for Predicting Great Salt Lake Levels. University of Utah, Salt Lake City, pp. 40–53.
Munroe, J.S., 2005. Glacial geology of the northern Uinta Mountains. In: Dehler, C.M., Pederson, J.L. (Eds.), Uinta Mountain Geology. Utah Geological Association Publication 33, pp. 215–234.
Munroe, J.S., Laabs, B.J.C. Glacial geologic map of the Uinta Mountains region, Utah and Wyoming. Utah Geologic Survey Open File Report, scale 1:100,000, in press.
Munroe, J., Mickelson, D., 2002. Last Glacial Maximum equilibrium-line altitudes and paleoclimate, northern Uinta Mountains, Utah, U.S.A. Journal of Glaciology 48, 257–266.
Munroe, J.S., Laabs, B.J.C., Shakun, J.D., Singer, B.S., Mickelson, D.M., Refsnider, K.A., Caffee, M.W., 2006. Latest Pleistocene advance of alpine glaciers in the southwestern Uinta Mountains, Utah, USA: evidence for the influence of local moisture sources. Geology 34 (10), 841–844.
Murray, D.R., Locke III, W.W., 1989. Dynamics of the late Pleistocene Big Timber Glacier, Crazy Mountains, Montana, U.S.A. Journal of Glaciology 35, 183–190.
Muzikar, P., Elmore, D., Granger, D.E., 2003. Accelerator mass spectrometry in geologic research. Geological Society of America Bulletin 115, 643–654.
Nelson, A.R., Millington, A.C., Andrews, J.T., Nichols, H., 1979. Radiocarbon-dated upper Pleistocene glacial sequence, Fraser Valley, Colorado Front range. Geology 7, 410–414.
Osborn, G.D., 1973. Quaternary geology and geomorphology of the Uinta Basin and the south flank of the Uinta Mountains, Utah. Ph.D. dissertation, Berkeley, University of California, 266 pp.
Oviatt, C.G., 1997. Lake Bonneville fluctuations and global climate change. Geology 25, 155–158.
Oviatt, C.G., 1994. Quaternary geologic map of the upper Weber River drainage basin, Summit County, Utah. Utah Geological Survey, Map 156, scale 1:50,000.
Owen, L.A., Finkel, R.C., Minnich, R.A., Perez, A.E., 2003. Extreme southwestern margin of the late Quaternary glaciation in North America – timing and controls. Geology 31, 729–732.
Peltier, W.R., Fairbanks, R.G., 2006. Global glacial ice volume and Last Glacial Maximum duration form an extended Barbados sea level record. Quaternary Science Reviews 25, 3322–3337.
Phillips, F.M., Zreda, M.G., Benson, L.V., Plummer, M.A., Elmore, D., Sharma, P., 1996. Chronology for fluctuations in Late Pleistocene Sierra Nevada glaciers and lakes. Science 274 (5288), 749–751.
Porter, S.C., Swanson, T.W., Finkel, R.C., Caffee, M., 2008. ^{36}Cl dating of the classic Pleistocene glacial record in the northeastern Cascade Range, Washington. American Journal of Science 308, 130–166.
Porter, S.C., Pierce, K.L., Hamilton, T.D., 1983. Late Wisconsin mountain glaciation in the western United States. In: Porter, S.C. (Ed.), Late-Quaternary Environments in the Western United States. The late Pleistocene, vol. 1. University of Minnesota Press, Minneapolis, pp. 71–111.
Putkonen, J., Swanson, T., 2003. Accuracy of cosmogenic ages for moraines. Quaternary Research 59, 255–261.
Putkonen, J., Connolly, J., Orloff, T., 2008. Landscape evolution degrades the geologic signature of past glaciations. Geomorphology 97, 208–217.
Refsnider, K.A., Laabs, B.J.C., Plummer, M.A., Mickelson, D.M., Singer, B.S., Caffee, M.W., 2008. Last Glacial Maximum climate inferences from cosmogenic dating and glacier modeling of the western Uinta ice field, Uinta Mountains, Utah. Quaternary Research 69, 130–144.
Refsnider, K.A., Laabs, B.J.C., Mickelson, D.M., 2007. Glacial geology of the Provo River drainage, Uinta Mountains, U.S.A. Arctic, Antarctic and Alpine Research 39 (4), 529–536.
Richmond, G.M., Fullerton, D.S., 1986. Summation of Quaternary glaciations in the United States of America. Quaternary Science Reviews 5, 183–196.
Rosenbaum, J.G., Heil Jr., C.W. The glacial/deglacial history of sedimentation in Bear Lake, Utah and Idaho. In: Rosenbaum, J.G., Kaufman, D.S. (Eds.), Paleoenvironments of Bear Lake, Utah and Idaho: Geological Society of America Special Paper, in press.
Shakun, J.D., 2003. Last Glacial Maximum Equilibrium-line Altitudes and Paleoclimate, Northeastern Utah. B.A. thesis, Middlebury, Middlebury College, 55 p.
Stone, J.O., 2000. Air pressure and cosmogenic isotope production. Journal of Geophysical Research, B, Solid Earth and Planets 105, 23,753–23,759.
Thackray, G.D., 2008. Varied climatic and topographic influences on Late Pleistocene mountain glaciation in the western United States. Journal of Quaternary Science 23, 671–681.
Thackray, G.D., 2001. Extensive early and middle Wisconsin glaciation on the western Olympic Peninsula, Washington, and the variability of Pacific moisture delivery to the northwestern United States. Quaternary Research 41, 265–277.
Thackray, G.D., Lundeen, K.A., Borgert, J.A., 2004. Latest Pleistocene alpine glacier advances in the Sawtooth Mountains, Idaho, USA: reflections of midlatitude moisture transport at the close of the last glaciation. Geology 32, 225–228.
Wilkins, D.E., Currey, D.R., 1997. Timing and extent of late Quaternary paleolakes in the Trans-Pecos closed basin, west Texas and south-central New Mexico. Quaternary Research 47, 306–315.
Zielinski, G.A., McCoy, W.D., 1987. Paleoclimatic implications of the relationship between modern snowpack and late Pleistocene equilibrium-line altitudes in the mountains of the Great Basin, western U.S.A. Arctic and Alpine Research 19 (2), 127–134.